CARBON NANOPARTICLES BASED POLYPROPYLENE NANOCOMPOSITES

by

Farzad Abdollahzadeh Bina

B.S., Mechanical Engineering, Tabriz Azad University, 2009

Submitted to the Institute for Graduate Studies in
Science and Engineering in partial fulfillment of
the requirements for the degree of
Master of Science

Graduate Program in Mechanical Engineering
Boğaziçi University

2017

ACKNOWLEGDEMENTS

I would like to express my deepest gratitude to my supervisor Assoc. Prof. Nuri Ersoy who has a great influence on me to pave the way for future advances. He advised and supported me under any conditions.

I am also thankful to my committee members, Assoc. Prof. Hakan Ertürk and Asso.Prof. Melih Papila for their comments and constructive critics.

I am grateful to my mother, Akram Gharghish, my father, Mahmoud Abdollahzadeh Bina, and sister, Farzaneh Abdollahzadeh Bina for their continuous support, encouragement and patience.

I would like to express a special thanks to my best friends Fatih Ertuğrul Öz and Onur Yüksel who did a great job giving very fruitful assistance along with technical hints.

I also appreciate to other friends and colleagues Dr. Kenan Çinar, Yakup Okan Alpay, Ayşenur Özdemir.

ABSTRACT

CARBON NANOPARTICLES BASED POLYPROPYLENE NANOCOMPOSITES

Although polymers have some advantages like easy processability, good chemical resistance, low cost, and low specific gravity as compared to metals and ceramic, they have disadvantages such as low strength, low modulus, low operating temperature, and low electrical and thermal conductivities. Therefore, to overcome these cons, this study investigates experimentally the property transformation of polypropylene by the addition of carbon based nano-scale particles, in particular graphene, as a second phase.

The study was carried out in three experimental steps in order to observe the effect of addition of carbon based nano-scale particles on the mechanical and electrical properties of the polypropylene matrix. First, carbon fibres were melt mixed with the polypropylene via melt mixing. Second, carbon black masterbatch were diluted at various ratios with polypropylene by melt mixing. Finally, graphene was melt mixed into the polymeric matrix and the mechanical and electrical properties of those composites and nanocomposites were measured and the results were discussed.

ÖZET

KARBON NANO-PARÇACIK TAKVİYELİ POLİPROPİLEN NANOKOMPOZİTLERİ

Polimerler kolay işlenebilirlik, iyi kimyasal direnç, düşük maliyet ve düşük özgül ağırlık gibi bazı avantajlara sahip olsa da metal ve seramik ile karşılaştırıldığında düşük mukavemet, düşük elastisite modülü, düşük çalışma sıcaklığı, düşük elektrik ve ısıl iletkenlik gibi dezavantajlara sahiptir. Bu nedenle, bu dezavantajları aşmak için, bu çalışmada ikinci faz olarak, karbon esaslı nano ölçekli parçacıklar ilave edilerek polipropilenin özelliklerinin dönüşümü araştırılmıştır.

Bu çalışma, karbon esaslı nano boyutlu parçacıklar eklenmesinin polipropilen matrisinin mekanik ve elektriksel özelliklerinde yol açtığı değişiklikleri gözlemek için üç aşamada gerçekleşmiştir. İlk olarak, karbon lifleri, polipropilen içine ektrüzyon prosesi ile karıştırılmıştır. İkinci olarak, karbon karası mastırbeç, eriyik karıştırma yöntemiyle polipropilen içinde çeşitli oranlarda seyreltilmiştir. Son olarak, grafen polimerik matris içerisine eriyik karıştırma yöntemi ile karıştırılmış ve bu kompozit ve nanokompozitlerin mekanik ve elektriksel özellikleri ölçülmüş ve sonuçları tartışılmıştır.

TABLE OF CONTENTS

ACKNOWLEGDEMENTS iii
ABSTRACT iv
ÖZET v
LIST OF FIGURES viii
LIST OF TABLES xiii
LIST OF SYMBOLS xv

1. INTRODUCTION 1

1.1. Literature Review 3
1.1.1. Carboneous Nanoparticles 3
1.1.2. Production of Expanded Graphite 5
1.1.3. Production of Graphene 6
1.1.4. Functionalization of Graphene 6
1.1.5. Reduction of Graphene Oxide 9
1.1.6. Effect of Carbon Nanoparticles on a Polymeric Matrix in terms of Mechanical Properties 11
1.1.6.1. Improvement of Mechanical Properties.. 12
1.1.6.2. Unbalanced Behaviour of Mechanical Properties.. 17
1.1.7. Effect of Carbon Nanoparticles on a Polymeric Matrix in terms of Electrical Conductivities 19
1.1.7.1. The Effect of Different Parameters on the Electrical Percolation Threshold 22
1.1.7.2. Effect of Production Methods on the Electrical Percolation Threshold.. 24
1.2. Problem Statement 33

2. EXPERIMENTAL WORK 35

2.1. Materials and Manufacturing 35
2.1.1. Materials 35
2.1.2. Equipment 36
2.2. Specimen Preparation 37

2.2.1. Carbon Fibre-Polyamide (CF-PA6) and Carbon Fibre-Polypropylene (CF-PP) Composites 38
2.2.2. Production of Carbon Black-Polypropylene (CB-PP) Nanocomposites 44
2.2.3. Production of Exfoliated Graphene Nanoplatelets-Polypropylene (xGnPs-PP) Nanocomposites 46
2.3. Testing 49
2.3.1. Tensile Strength 49
2.3.2. Melt Flow Index Measurements 51
2.3.3. Scanning Electron Microscopy (SEM) 51
2.3.4. Thermogravimetric Analysis (TGA) 52
2.3.5. Electrical Property Measurements 53
3. RESULTS AND DISCUSSIONS 54
3.1. Mechanical Properties 54
3.1.1. CF-PA6 Composite 55
3.1.2. CF-PP Composites 57
3.1.3. CB-PP Nanocomposites 60
3.2. Rheological Properties 64
3.2.1. Melt Flow Index 64
3.3. Scanning Electron Microscopy (SEM) 66
3.4. Thermogravimetric Analysis (TGA) 67
3.5. Electrical Property Measurements 69
4. CONCLUSION AND FUTURE WORK 74
REFERENCES 79

LIST OF FIGURES

Figure 1.1. Graphene is a 2D building material for carbon materials of such a 0D buckyballs, 1D carbon nanotubes or 3D graphite. 3

Figure 1.2. Scanning electron microscopy view of a typical Carbon Black aggregate consisting of fused primary particles. 5

Figure 1.3. SEM image of the expandable graphite. 5

Figure 1.4. Graphite oxide structural model proposed by Klinowski *et al.* 8

Figure 1.5. Increase of the average conductivity of graphene films with the temperature increase. 10

Figure 1.6. Photographs of aqueous dispersion of graphene oxide before (a) and after (b) being reduced by hydrazine hydrate. 14

Figure 1.7. XRD pattern of pristine graphite, graphite oxide (GO), and chemically reduced graphene oxide (GNs). 15

Figure 1.8. XRD pattern of neat PP and its nanocomposites with effective GNs contents of 0.2, 0.5, 1.0, 2.0, 3.0 wt.% 15

Figure 1.9. SEM images of PP nanocomposites containing (a) 1.0 wt.%, (b) 1.5 wt.%, and (c) 2.0 wt.% of GNs content from left to right 15

Figure 1.10. Tensile strength and modulus of elasticity curves with different GNs contents. 16

Figure 1.11. Tensile strength and elaongation at break curves with different graphene contents. 18

Figure 1.12. SEM images of (a) PET/graphene nanocomposite (0.03 wt.%) and (b) PET/graphene nanocomposite (0.07 wt.%). 18

Figure 1.13. Schematic of conductive network formation in a CPC. 19

Figure 1.14. The approximate range of electrical conductivity covered by CPCs.... 20

Figure 1.15. Simplified diagram of the electronic band structure in the band theory. 22

Figure 1.16. The electrical conductivity as a function of the CB content for the CPC samples in the parallel and perpendicular directions. The insert shows a log-log plot of the conductivity as a function of $\varphi - \varphi c$ for the CPC. 24

Figure 1.17. Conductivity of the PP composites with different types of fillers versus filler loading. 25

Figure 1.18. Electrical percolation thresholds of graphene/polymer nanocomposites according to processing strategy. 26

Figure 1.19. Effect of carbon based fillers and annealing (30 min at 190°C) on the electrical conductivity of PP composites. 27

Figure 1.20. Effect of CNT and annealing (30 min at 190°C) on the electrical conductivity of PP/TrGO/CNT hybrid composites. Hybrid composites with 1.0 vol.% of TrGO (left) and hybrid composites with 2.0 vol.% of TrGO (right). 28

Figure 2.1. Scanning Electron Microscopy of graphene nanoplatelets. 36

Figure 2.2. Raman spectroscopy- Graphene nanoplatelets. 36

Figure 2.3. The schematic of the twin screw compounding extruder..... 40

Figure 2.4. Different types of modular screws assembled on high torque splined shafts (conveying elements, melting and mixing elements, and intake element from left to right). 40

Figure 2.5. Screws configuration for CF based PP and CF based PA6 composites. 40

Figure 2.6. Schematic of the screw configuration and extruder configuration for compounding CF-polymer composites. For temperature profile, refer to table 2.1. 40

Figure 2.7. The schematic drawing of a typical injection molding machine. 41

Figure 2.8. Melt blending temperature profile per each zone with respect to the nanofillers loading. 41

Figure 2.9. Injection molding temperature profile per each zone with respect to the nanofillers loading..... 42

Figure 2.10. Types of modular screws assembled on high torque splined shafts (conveying element, mixing element, melting and mixing elements, intake element, and back pressure element from left to right). 46

Figure 2.11. Screws configuration for CB based PP nanocomposites. 46

Figure 2.12. Closed-circuit ultrasonication system. 47

Figure 2.13. Screws configuration for xGnPs-PP nanocomposites. 48

Figure 2.14. Tensile test set-up. 49

Figure 2.15. Schematic drawing of the tension test specimen. 50

Figure 2.16. Melt Flow test set-up located at Bogaziçi Mechanical Lab.. 51

Figure 2.17. Philips XL30 ESEM system. 52

Figure 2.18. Electrical percolation thresholds of graphene/polymer..... 53

Figure 2.19. Grinded samples ready to be silver coated. 53

Figure 3.1. Typical stress-strain curves for polymers, reproduced from ISO 527-1 standard. 55

Figure 3.2. Stress-strain graphs of PA6 samples. 56

Figure 3.3. Stress-strain graphs of PA6/10CF samples. 57

Figure 3.4. Stress-strain graphs of PP samples. 58

Figure 3.5. Stress-strain graphs of 20CF/MA-g-PP/PP samples. 59

Figure 3.6. Stress-strain graphs of CF-PP and CF-PA6..... 60

Figure 3.7. Stress-strain curves of CB-PP nanocomposites and neat PP..... 61

Figure 3.8. Stress-strain graphs of 4xGnPs-PP samples. 62

Figure 3.9. Stress-strain graphs of 8xGnPs-PP samples. 63

Figure 3.10. Stress-strain graphs of CB-PP and xGnPs-PP nanocomposites. 64

Figure 3.11. Scanning electron microscopy of different nanocomposites with various nanofiber fractions magnified at 5000x. 67

Figure 3.12. TGA curves of different nanocomposites. 68

Figure 3.13. Real impedance (Z') vs. frequency of xGnPs/PP nanocomposites as a function of graphene weight fraction. 71

Figure 3.14. Real impedance (Z') vs. frequency of CB/PP nanocomposites as a function of graphene weight fraction. 72

LIST OF TABLES

Table 1.1. CPC applications with their required range of electrical conductivity. 20

Table 1.2. Electrical properties of polymer/GNP nanocomposites. 29

Table 1.3. Properties of single layer graphene. 34

Table 2.1. Temperature profiles (Extrusion & injection molding process). 42

Table 2.2. Process parameters (Extrusion & injection molding)..... 43

Table 2.3. Ultrasonication and mechanical mixer process parameters for surfactant assessment. 47

Table 2.4. Parameters of the tensile test according to the ISO527. 50

Table 2.5. Specimen Dimensions. 50

Table 3.1. Mechanical properties of neat PA6 Material. 56

Table 3.2. Mechanical properties of 10CF/PA6 composite. 57

Table 3.3. Mechanical properties of neat PP 58

Table 3.4. Mechanical properties of 20CF/MA-g-PP/PP composite. 59

Table 3.5. Mcehnaical properties of 4xGnPs-PP nnaocomposites. 62

Table 3.6. Mechanical properties of 8xGnPs-PP % nanocomposites 63

Table 3.7. Melt Flow indexes of nanocomposites according to the ASTM-D1238 [89]. 65

Table 3.8. Thermal degradation parameters obtained by TGA of nanocomposites. 68

Table 3.9. Conductivity of the nanocomposites with different fibre loading in various frequencies 73

LIST OF SYMBOLS

A	Surface Area
e	Electric Field
E	Charge of Electron
g	Gram
J	Current Density
L	Liter
Ne	Number of Electrons
R	Resistance
T	Thickness
μ	Electron Mobility
ρ_v	Volume Resistivity
σ	Electrical conductivity
°C	Celsius

LIST OF ACRONYMS / ABBREVIATIONS

CB	Carbon Black
CNT	Carbon nanotube
CNTs	Carbon nanotubes
CO	Carbon monoxide
CO_2	Carbon dioxide
CPCs	Electrically conductice polymer composites
DAH	1,6-diamiohexane
DCB	1,2-dichlorobenzene
EG	Expanded graphite
EVA	Polyethylene-co-vinyl acetate
FESEM	Field emmision scanning electron microscopy
GA	Gum Arabic
GnPs	Graphene nanoplateletes
GNs	Graphene nanosheets
GO	Graphite Oxide
HCl	hydrogen chloride
HI	hydroiodic acid
H_2O_2	hydrogen peroxide
iPP	isotactic polypropylene
iPP-FR	Fire retardant isotactic polypropylene
$KMnO_4$	potassium permanganate
LLDPE	Linear low density polyethylene
MWCNTs	Multi walled carbon nanotubes
$NaBH_4$	sodium borohydride
N_2H_2	Diazene
NMP	N-methyl-pyrrolidone
PA6	Polyamide-6
PA12	Polyamide 12
PC	Polycarbonate

PE	Polyethylene
PET	polyethylene terephthalate
PHR	Part hundred of rubber
PVP	Polyvinylpyrrolidone
SAN	Styrene Acrilonitrile
SDS	Sodium Dodecyl Sulphate
SEM	Scanning Electron Microscopy
SEBS-g-MA	styrene-ethylene-butylene-styrene-g-maleic anhydride
TEM	Transmission Electron Microscopy
THF	Anhydrous stabilized tetrahydrofuram
TrGO	Thermally reduced graphite oxide
xGnPs	Exfoliated graphene nanoplatelets
XRD	X-Ray Diffraction

1. INTRODUCTION

Traditional materials cannot meet the increasing technological demands to produce faster, more economical, stronger machines and devices; hence, engineers are looking for new materials and manufacturing technologies. Nanocomposites are one of the most advanced types of emerging materials. Due to the nature of manufacturing procedures and investment costs, total cost for nanocomposite materials is higher than traditional materials. In addition, insufficient information about process parameters and their effects on final product geometry also increase the cost due to scrapped products. These are acceptable drawbacks since the aforementioned materials have many favourable properties. On the other hand, higher cost is tried to be decreased with considerable research effort in order to strengthen the advantages of nanomaterials over traditional materials.

Despite their high cost and processing difficulties, due to their intrinsic potentials, nanomaterials have drawn considerable attention in industrial applications. For example, considering the fact that the automotive and aerospace industries are one of the leading and the most populated areas of research, nanocomposites constitute the basis for applications such as door handles, engine covers, belt covers, and mirror housing on various types of vehicles. Besides, deicing, and conductive coatings in aerospace and wind turbine blades, packaging, solar cells, fuel tanks, fuel cells, power tool housing, cover for portable electronic equipment, gas barrier for plastic bottles, products with low flammability have already taken into account [1]. The large number of studies and publications on nanocomposites in the last two decades indicate the importance and great potential of these materials [1].

Furthermore, nanocomposites are the materials in which at least one of the phases demonstrates nanometer dimension. They have been brought about a solution against the constraints of microcomposites and monolithic materials. Surface area/volume ratio of the reinforcing materials should be taken into account in order to conceive the structure-property relationships. In other words, surface area per volume ratio has an inverse relationship to the

diameter of materials such that the greater the surface area per unit volume, the smaller the diameter [2]. As the dimension of the composite materials reach to the nanometer scale, the interaction at phase interface is increased, which results in high properties.

Also, to produce nanocomposites with various types of matrices, three main methods have already been examined: First, in situ polymerization method in which the nanoparticles are first injected into the solvent to achieve a stable suspension; then, the polymer is added followed by incorporation of some interfacial agents to increase the level of suspension`s stabilization state; finally, polymerization is completed followed by the removal of the solvent. This method was pioneered by Toyota, and then applied to different polymeric matrices [3]. Second, solvent blending method in which a polymer is filled with nanoparticles such that an appropriate solvent, capable of dissolving polymer and swelling the nanoparticles, is chosen. Then, mechanical mixer and/or ultrasonication method is used to obtain the suspension of polymer and nanoparticles followed by the removal of solvent either by evaporation or by precipitation in a non-solvent [4]. Finally, melt mixing technique is the method in which polymer and the nanoscale materials are mixed together through the combination of heat and pressure in order to force the nanocomposite to the die with the uniform shape and homogeneity [5].

Therefore, because of the graphene's exceptional mechanical and physical properties, its abundance and affordability compared to other carbon nanoparticles such as carbon nanotubes and fullerenes, it was chosen in this study as the reinforcing materials in the polymeric matrices, and its effect on different polymeric matrices was summarized and reviewed. In addition to choosing the cost-effective and multifunctional nanocarbon particle, good processing methods are necessary which guarantee the high quality of exfoliation of graphene nanoplatelets, dispersion, and distribution homogenously with ability of being produced in continuous mass production areas. In this regard, solution mixing followed by ultrasonication is employed to exfoliate the graphite nanoplatelets. Later, melt mixing, which is an appropriate process for mass production industries, is used to disperse and distribute exfoliated graphene nanoplatelets in the polymeric matrix uniformly resulting in the considerable increase in mechanical and electrical properties.

1.1. Literature Review

1.1.1. Carboneous Nanoparticles

There are various kinds of carbonaceous nanofillers that have already been found by scientists, and they have been categorized based on their dimensions- 0-Dimensional (0D) fullerenes or buckyballs, 1-Dimensional (1D) carbon nanotubes, 2-Dimensional (2D) grapehe, and 3-Dimensional (3D) are spherical and cubical nanoparticles such as carbon black and graphite. (Figure 1.1).

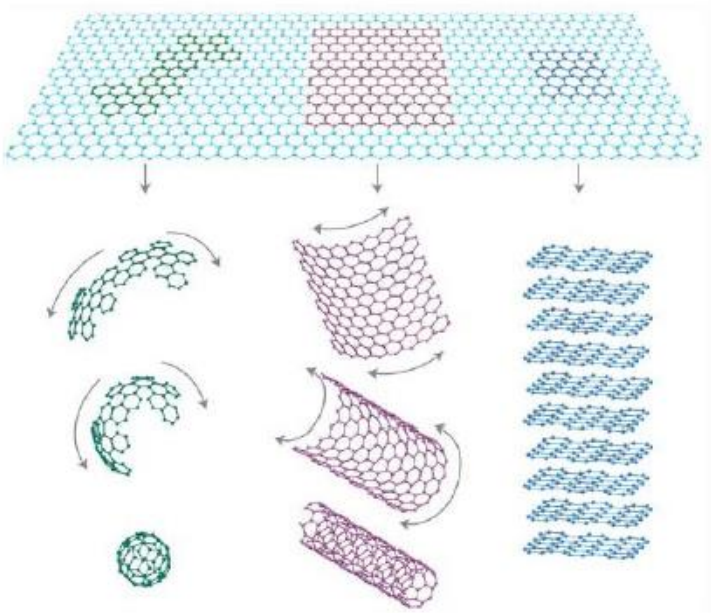

Figure 1.1. Graphene is a 2D building material for carbon materials of such a 0D buckyballs, 1D carbon nanotubes or 3D graphite. [6]

Graphene, on one hand, is the two-dimensional single atom thick sheet composed of carbon structure in the form of honeycomb is the building block for all sp^2 hybridized carbon allotropes, and it is the basal plane for graphite (3D), CNTs (1D), and fullerene (0D) shown in figure 1.1 [7-10]. Graphite is entirely constituted of carbon atoms and 1mm-thick graphite has approximately 3 million graphene layers.

Graphene can be described as the miracle material encompassing different mechanical and physical (thermal- electrical) properties. From those properties, 1 TPa Young's modulus, 130 GPa tensile strength, 5000 W/mK thermal conductivity, 2630 m^2/g specific surface area, 200000 cm^2/vs carriers mobilities, and 6000 S/cm electrical conductivity, can be named. In fact, it conducts electricity better than copper as well as its strength is higher than steel, and it is as flexible as rubber.

Carbon nanotubes, on the other hand, are constituted of graphene sheets rolled in cylindrical shape with hemisphere of fullerenes at both ends. They are classified as single walled carbon nanotubes (SWCNTs) which have a diameter close to 1 nanometer with length per diameter ratio reaching to millions, and multiwalled carbon nanotubes (MWCNTs) which are formed by wrapping a single layers of graphene into concentric cylinders and those cylinders' interlayer distance is 3.4 A° similar to the value which graphite has. They have high Young's modulus in the direction of the nanotube's axis, their hollow structure that can encapsulate the foreign substances such as metal, water, and molecular oxygen and creates different properties other than their bulk forms such as bulk water. They also are as half dense as aluminium and have tensile strength 20 times that of high strength alloys. Scientists have already found that nanotubes demonstrate extraordinary mechanical properties such as 1TPa tensile modulus, 50-150 GPa tensile strength, and strain at break in excess of 5%. The reason that distinguishes Carbon nanotubes and graphene from other conventional fillers like carbon black is their high aspect ratio (L/D).

Carbon black is another form of carbonaceous nanoparticle and can be described as very fine particulate aggregate that is produced by partial combustion or thermal decomposition of gaseous or liquid hydrocarbons under controlled conditions. Its physical feature is that of a finely black pellet or powder, and its high specific surface area, particle size and structure, conductivity, and colour have led it to be widely used in tires, rubber, plastic products, printing inks, and coating.

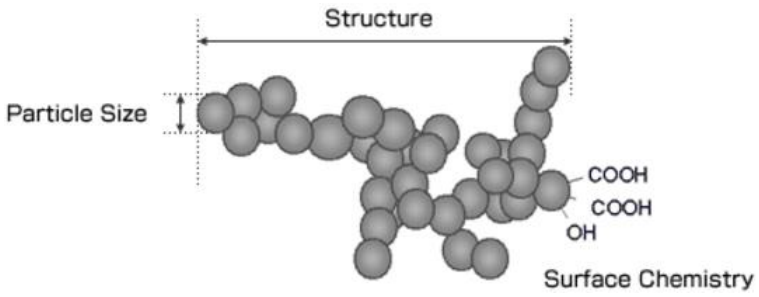

Figure 1.2. Scanning electron microscopy view of a typical Carbon Black Aggregate consisting of fused primary particles [11].

1.1.2. Production of Expanded Graphite

Crystalline graphite is composed of stacks of parallel planes of carbon atoms. Since there is no covalent bonding between accumulated graphene layers, other molecules can be placed between them. This process, known as intercalation, is necessary to produce the expandable graphite. A wide range of intercallants are used such as halogens, alkali metals, sulfate, nitrate, various organic acids, aluminium chloride, ferric chloride, other metal halides, arsenic sulfide, thallium sulfide, etc. Among them, sulfric acid is commercially used within the intercallation process. As the intercallated graphite is exposed to heat or flame, the embedded molecules decompose to generate gas resulting in the expansion of graphite layer planes. The expanded graphite flake is a low-density, non-burnable, highly thermally insulative that can reflect about 50% of radiated heat and it has been illustrated in Figure 1.3 [12, 13].

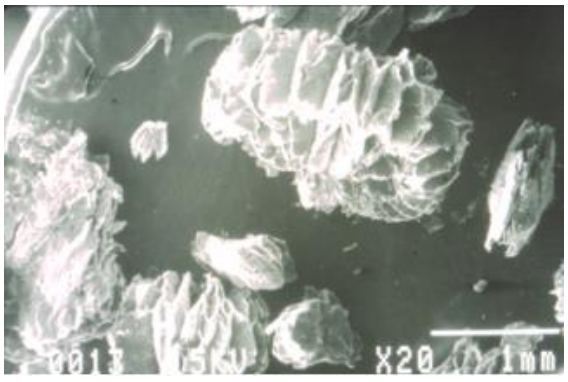

Figure 1.3. SEM image of the expandable graphite [13].

1.1.3. Production of Graphene

Many studies have been done regarding the techniques of the production of the single layer graphene and graphite nanoplatelets (GNPs). Production of the single layer graphene can be categorized into three main methods: (i) micromechanical cleavage which is the graphite peeling against other flat surfaces in order to get the single layer of graphene; (ii) the solution based reduction of graphene oxide method in which the graphite oxide is used as a medium to acquire stable graphene dispersion in a solvent; (iii) epitaxial graphene growth method in which graphene is treated by silicon carbide wafers at high temperature. The first two methods are known as "top-down" methods since they utilize a natural precursor (graphite) to obtain graphene, whereas the last method is a "bottom-up" approach, since graphene is synthesized by using chemical vapor deposition.

In solution based methods, which is the most promising method to produce mass graphene nanoplatelets (GNPs), graphitic nanofillers composed of stacked 2D graphene sheets are produced by three main methods: (i) cationic surfactant mediated exfoliation of graphite into graphene nanoplatelets in which mild ultrasonication of highly ordered pyrolytic graphite in the presence of acetic acid and cationic surfactant cetyltrimethylammonium yielded graphene nanoplatelets which made a stable colliodal suspension in organic solvent such as N,N-dimethyl formamide [14], (ii) high yield purification and production of graphene nanoplatelets by Gum Arabic assisted physical sonication in the water [15], (iii) Preparation of graphene flakes in the water by the surfactant sodium cholate assisted by low power sonication for long times (up to 400h) [16].

1.1.4. Functionalization of Graphene

The literature review was divided into two main categories: (i) studies which have been focused on the effect of the functionalized graphene based polymeric nanocomposites in terms of mechanical properties, (ii) studies which have been investigated the effect of functionalized graphene based polymeric nanocomposites in terms of electrical conductivity.

Increasing popularity of nanocomposites raised the necessity to understand the effect of nanomaterials' surface characteristics on final product rigorously. Therefore, in the last decades, functionalization of the surfaces of nanoscale materials has attracted much attention

from research teams working on nanocomposites. As far as the functionalization of nanocarbon materials are concerned, there are Van der Waals forces between the layers of graphene, which facilitates the reaggregation of the exfoliated layers, but hinders their dispersion throughout the polymer. In addition, due to the graphene layers` surface inertia, its integration with polymers is a problematic issue. The aforementioned drawbacks contribute to the presence of stress concentration regions leading to the insufficient load transfer, which affects the products` properties. Reason behind the nanocarbon materials` functionalization is to provide the better property transformation of the filler to the matrix. In other words, to achieve good mechanical and electrical properties, nano-carbon materials should be distributed and dispersed homogenously throughout the polymeric matrix. Therefore, among the most applicable functionalization methods, oxidation and reduction processing of the nano-carbon materials is the most invaluable and versatile technique.

In this respect, pure graphite layers are being oxidized and then either chemically or thermally reduced in order to be better dispersed in the organic solvents or water. In fact, oxidation of graphite leads to the graphite oxide coumpound, which will have the functional groups such as carboxyl, hydroxyl, carbonyl, and epoxide groups on the basal or edge planes, as depcited in Figure 1.4. The functional groups existed on the graphite oxide plane will result in the formation of stable colloidal dispersion due to GO's hydrophilicity. On the contrary, electrical properties of the GO can be compromised with an increase in hydrophilicity during the oxidation process due to the transferring of carbon atoms from sp^2-hybridized geometry to sp^3-hybridized geometry. To deal with this issue, graphite oxide has to be reduced to eliminate most of the oxygen containing functionalities so that the aromatic graphene networks are recovered. The oxidation process can itself compromise the electrical conductivity of the materials, but applying the reduction process can improve it.

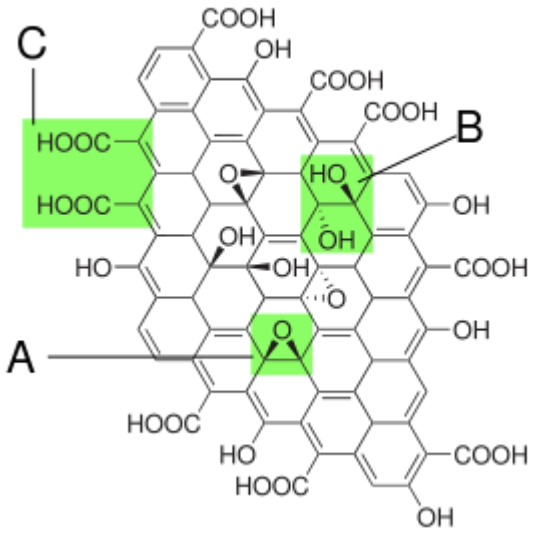

Figure 1.4. Graphite oxide structural model proposed by Klinowski *et al*. [17].

Brodie [18] used the oxidizing agents such as potassium chlorate such that 10g of graphite was dispersed in 250 ml concentrated nitric acid followed by adding 5 g $NaNO_3$ (sodium nitrate). The obtained suspension was put in the ice bath followed by adding 30 g $KMnO_4$ within 5h; the suspension was quenched in a 500 ml ice water plus some milliliters H_2O_2 in order that the excess $KMnO_4$ to be eliminated. Later, the suspension was washed several times with HCl and water and then dried with lyophilization. Finally, the dried GO was rapidly heated up to 600℃ using metallic reactor to obtain Thermally Reduced Graphene Oxide (TrGO).

In a different but similar technique, Staudenmair [19] used multiple feeding methods instead of single feeding of potassium chlorate, applied by Brodie, in the present of sulfric acid without using the concentrated fuming nitric acid. Later, Hummers and coworkers [20] introduced new method containing potassium permanganate along with concentrated sulfuric acid and sodium nitrate which is nowadays one of the most common techniques in oxidizing the graphite flakes and the whole process takes less than two hours to be completed at temperature below $45°C$. Graphite Oxide (GO) encompasses several functional groups such as carboxyl, hydroxyl, and carbonyl which can pave the way for tranforming to other functionalities through acylation and esterification [21, 22].

1.1.5. Reduction of Graphene Oxide

Since the aforementioned oxidation methods harm the sp^2 bonding networks resulting in reduction in the electrical conductivity, both graphene oxide and graphite oxide are reduced to recover the π-network. Also, the reduction methods have proven that the reduced graphene oxide has much more similarity to pristine graphene. In this respect, reduction strategies can be categorized into two main groups: chemical reduction, and thermal reduction. Given the thermal reduction, GO must be heat-treated. At first, the GO was undergone rapid heating (>2000 ℃$/min$) to be exfoliated and the graphene was created. In fact, the exfoliation method is the sudden expansion of CO or CO_2 gases placed between the graphene sheets, and the rapid heating causes the oxygen containing functional groups bonded on the carbon planes to be decomposed and generates the huge pressure between the stacked layers due to the formation of the gases.

Nevertheless, the process only produces small size and wrinkled graphene sheets since the decomposition of the oxygen containing functional groups eliminates the carbon atoms from the carbon plane affecting the electronic characteristics of the product. Alternatively, exfoliation of the graphite oxide in the liquid phase turns out to constitute graphene sheets with large lateral sizes, and this reduction is implemented by annealing in either inert or reducing atmosphere [23]. In this respect, heating temperature hugely influences the effect of reduction on GO such that Schniepp *et al*. [24] examined the effect of different temperatures- 500℃ & 750℃- over the variability of C/O ratio and found that it rises by the increase in temperature. In another study, Li *et al*. [25] proved that the good reduction of GO is achieved by higher temperature. Wang *et al*. [26] demonstrated the electrical conductivity of the GO is increased by rising the temperature from 500℃ in which the electrical conductivity value was 50 $S/_{cm}$ to 700℃ and 1100℃ in which the electrical conductivity values were measured 100 $S/_{cm}$ and 550 $S/_{cm}$ [Figure 1.5], respectively.

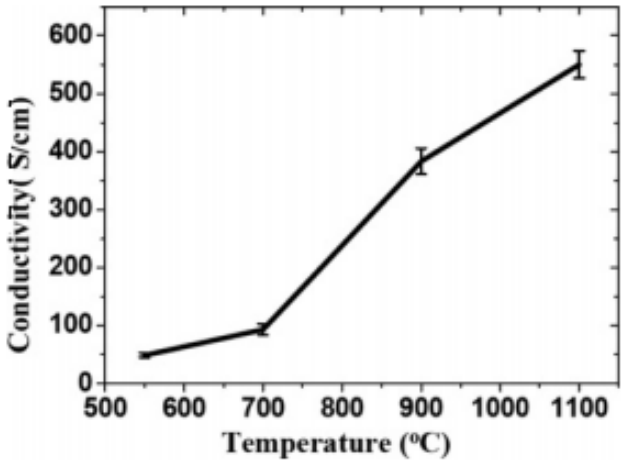

Figure 1.5. Increase of the average conductivity of graphene films with the temperature increase. [26].

Chemical reduction of the GO, on the other hand, is very simple, but it usually produces graphene-like film demonstrating the relatively low C/O ratio and considerable amount of residual functional groups. Actually, the technique takes advantage of using some reducing reagents such as hydrazine, sodium hydride, sodium borohydride and lithium aluminium hydride, etc. In fact, eliminating oxygen functional groups from GO is carried out by the reducing reagents. Stankovich *et al*. [27] found that hydrazine hydrate is the best reducing agent in producing very thin graphene sheets. Besides, some other studies [28-33] proved that the hydrazine can be a good chemical option in reducing the GO which would also paves the way for mass-production of Graphene even though there are some studies [27, 34, 35, 36] pointing out that the use of hydrazine would give rise to the high sheet resistance. Moreover, metal hydrides such as lithium and aluminium are the influential reducing agents in organic chemistry, but their reactivity with water vary from slight to very strong reaction. In this respect, Shin *et al*. [37] investigated the reduction effect of $NaBH_4$ on GO and found that sheet resistance of GO film is much lower than the one reduced by N_2H_2which can be attributed to the creation of C-N groups acting as donors in making up for the hole carriers in reduced graphite oxide. Using $NaBH_4$ leave some alcohol, epoxy groups, and carboxylic acids after being reduced although the reduction process eliminates C=O species. To solve this issue, Gao *et al*. [38] suggested an extra dehydration method employing sulfuric acid to reduce further the GO improving the electrical conductivity and C/O ratio. Fernandez-Merino *et al*. [31] found that the vitamin C can be a good substitution for both N_2H_2 and

$NaBH_4$ which proves that the same conductivity level is achieved with no toxicity. Further, Pei *et al*. [39] and Moon *et al*. [40] investigated the effect of HI as an another reducing material for GO and reported that the C/O ratio, conductivity, flexibility, and tensile strength is improved in comparison with the hydrazine and sodium borohydride reduced GO.

1.1.6. Effect of Carbon Nanoparticles on a Polymeric Matrix in terms of Mechanical Properties

Mechanical performance of the carbon nanoparticles based polymer nanocomposites is completely dependent both on the dispersion of filler in nanocomposite, which specifies the specific interfacial area, and the interfacial strength, which manages the stress transfer. Besides, if the interfacial region is stronger than the matrix, then the matrix fails, and if the matrix is stronger than the interfacial area, then the debonding may start across the interface. So, the integration of both filler and matrix must be optimized throughout the interface. Moreover, nano-scale carbon particles tends to agglomerate rapidly since there are Van der Waals forces between the layers and this prohibits the transfer of good mechanical properties from filler to polymeric matrices. Therefore, development of more advanced production methods can improve the dispersion and intercalation of polymer chains into multilayer structures in order to improve the mechanical performance of nanocomposites by preventing the graphene sheets from being agglomerated. In this respect, interface can be modified by mutating the surface of the graphene sheets [41], which also contribute to its dispersion into organic solvent and avoid restacking of layers. To better understand the effects of graphene nanoplatelets in the polymeric matrices, different studies have already been carried out, and classified into two groups: [42]: (i) Mechanical properties were improved, (ii) mechanical properties were improved up to the peak value at a critical particle concentration, and then went down with further particle loading. The second one was often considered as an ineffective dispersion at higher loading of nanoparticles resulting in more stress concentration sites and weak interfacial interaction. In this framework, mechanical characteristics of nanocomposites that were mostly focused on are tensile strength, modulus of elasticity, and strain at break.

1.1.6.1. Improvement of Mechanical Properties. Production of nanocomposites with enhanced mechanical properties is difficult. In fact, large interfacial region, dispersion of the nanofillers, and strong interfacial bonding are required to have the nanocomposites produced with high mechanical properties. Also, it can be said that existence of any kinds of interactions such as hydrogen bonding, van der waals forces, covalent and π-π bondings can anticipate the enhanced mechanical properties. Few studies have shown improvements of the mechanical properties such as elastic modulus, elongation at break, toughness, and tensile strength using various manufacturing techniques; some used in situ polymerization technique. Wang *et al*. [43] produced graphene reinforced polyvinyl alcohol (PVA) composite film by using graphene nanosheets and graphene oxide in an aqueous solution of PVA. Comparing graphene nanosheets/PVA with graphene oxide/PVA nanocomposites, it was found that graphene nanosheets/PVA nanocomposite with 0.5 wt.% graphene content demonstrated an increase in the mechanical characteristics at least two times as much as the graphene oxide/PVA nanocomposite. The resulting nanocomposites showed up to 212% increase in the tensile strength and 34% enhancement in the strain at break at 0.5 wt.% graphene content.

Similarly, Liang *et al*. [44] manufactured graphene oxide/PVA nanocomposites using simple and eco-friendly material such as water. It was inferred that the hydrophilicity of PVA as well as the existence of functional groups in the structure of graphene oxide led to better dispersion and interfacial interaction in the nanocomposite resulting in property enhancements at very low filler loading. They also found that a 76% increase in the tensile strength and a 62% improvement of modulus of elasticity can be achieved with 0.7 wt.% graphene content. In other words, hydrogen bonds, formed at the interface of graphene and PVA, contributed to better stress transfer across the interface. Zhao *et al*. [45] prepared the graphene based polyvinyl alcohol (PVA) nanocomposite films using in situ polymerization in the presence of compatibilizer. By adding graphene oxide into PVA aqueous solution stabilized by sodium dodecylbenzenesulfonate (SDBS) and reducing the graphene oxide thermally to the graphene nanosheets, they found that the mechanical properties of the nanocomposite film were improved significantly. In fact, 150% improvement in the tensile strength and approximately 10 times increase of the Young's modulus were reached at 1.8 vol.% graphene content. In addition, they conceieved that there is a critical point named mechanical percolation after which nanocomposite behaviour is changed.

Moreover, melt mixing method was another type of method applied to produce the nanocomposite. Achaby *et al*. [46] investigated and compared the mechanical properties of the graphene nanosheets (GNs)/high density polyethylene (HDPE) with the multi walled carbon nanotubes (MWCNTs)/HDPE nanocomposite with different nanofiller loading. GNs were obtained by oxidizing the graphite using Hummers' method and sonication. Then, the graphene oxide was reduced by hydrazine hydrate aimed at deoxygenation of graphite oxide followed by filteration, washing, and drying. MWCNTs, on the other hand, were used as received without any modification. They found that the GNs/HDPE nanocomposites have better mechanical properties than MWCNTs/HDPE nanocomposites. The tensile strength and Young's modulus of GNs/HDPE nanocomposite were increased at 3.0 wt.% GNs content about 72% and 81%, respectively. At 3.0 wt. % loading of MWCNTs in the HDPE matrix, on the other hand, nanocomposite demonstrated increases both in the tensile strength and in the modulus of elasticity about 54% and 59%, respectively. In fact, they attributed high performance of GNs/PE nanocomposite to the graphene nanosheets' high specific surface area, large aspect ratio, and 2D structure. Inuwa *et al*. [47] carried out a research regarding the effects of exfoliated graphite nanoplatelets on the blends of polypropylene and polyethylene terephthalate matrices. In this regard, polypropylene and polyethylene terephthalate were mixed by styrene-ethylene-butylene-styrene-g-maleic anhydride (SEBS-g-MAH) as a compatibilizer that had been proven by previous studies [48], and then as received exfoliated graphite nanoplatelets were dispersed in the polymeric matrix. They found that the uniform dispersion of graphite nanoplatelets across the polymeric matrix led to about 34% increase in the tensile strength, 41% increase in Young's modulus and 55% increase in the impact energy at 3.0 phr nanofiller loading.

Furthermore, some researchers employed two-step production method such as solution mixing and melt mixing. Achaby *et al*. [49] examined the effects of GNs on the polypropylene and found that the tensile strength and the modulus of elasticity of the resulting nanocomposite were increased up to 81% and 100% at 3.0 wt. % GNs content, respectively. Functionalization of graphite by Hummers' method followed by hydrazine hydrate reduction strengthened the interfacial bonding and dispersion. GNs was obtained by reducing the graphene oxide chemically and the graphite oxide powder was dispersed in the distilled water followed by sonication. Meanwhile, it was noticed that the graphite oxide suspension gradually turned into yellow-brown solution indicating the formation of

graphene oxide nanosheets. Finally, graphene oxide nanosheets were reduced by the hydrazine hydrate and the suspension's colour turned into black and GNs were achieved as shown in figure 1.6.

Figure 1.6. Photographs of aqueous dispersion of graphene oxide before (a) and after (b) being reduced by hydrazine hydrate [49].

To understand the complete exfoliation of graphene nanosheets, they conducted the x-ray experiments shown in Figure 1.7 and 1.8, which allowed them to find out the interlayer distance between graphite sheets and the exfoliation state of graphene. As shown in figure 1.7, for pristine graphite, a strong sharp reflection at $2\theta=26.23^{o}$ was observed indicating the interlayer distance 0.34 nm between graphite planes. After oxidation, the interlayer distance was increased to 0.9 nm proving the existence of oxygen-containg groups between graphite layers. Aside from shifting the angle to the left, the characteristic peak was widened due to the decrease in the crystallites sizes. As long as any secondary peaks did not occure, the complete oxidation of graphite was done. GNs, finally, proved the high level of exfoliation and chemical reduction lacking any considerable peaks. Moreover, the x-ray results regarding graphene nanosheets with different weight fractions in the polyopropylene shown in Figure 1.8 are compared with neat polypropylene and good exfoliation of graphene nanosheets was confirmed. Scanning electron microscopy (SEM) results shown in figure 1.9. demonstrated reasonable uniform dispersion of GNs indicating good interactions between GNs and polypropylene matrix. Overall, the aforementioned assessments of achieving the rational test results were corresponded to good mechanical properties such as tensile strength and modulus of elasticity with the increases in the nanofiber contents shown in figure 1.10.

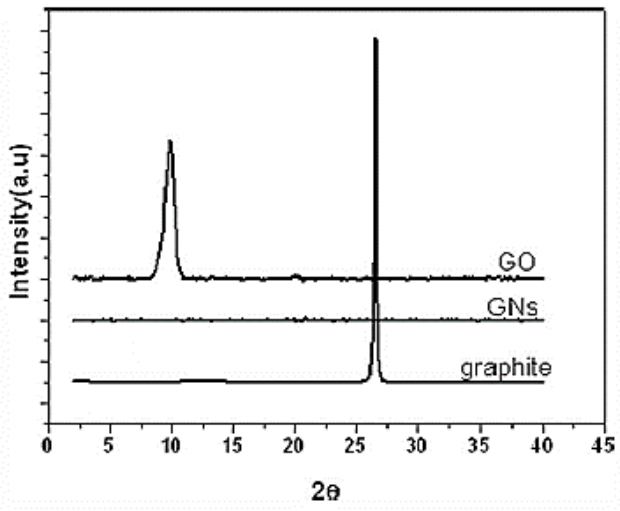

Fiurex 1.7. XRD pattern of pristine graphite, graphite oxide (GO), and chemically reduced graphene oxide (GNs) [49].

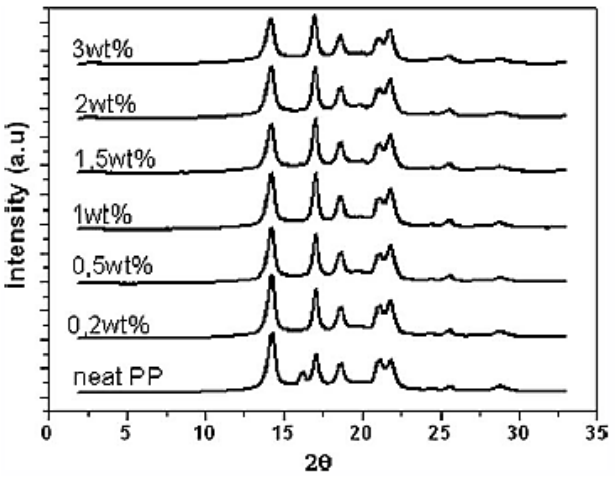

Figure 1.8. XRD pattern of neat PP and its nanocomposites with effective GNs contents of 0.2, 0.5, 1.0, 2.0, 3.0 wt.% [49].

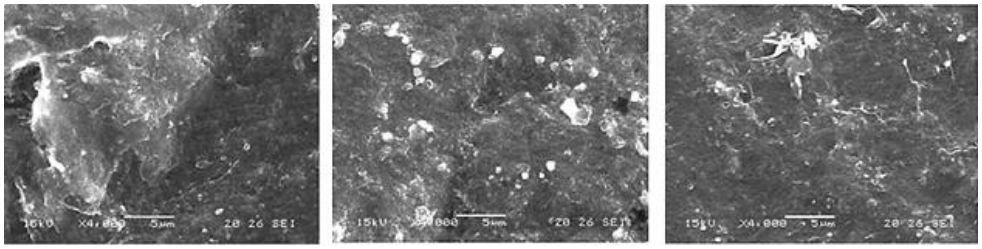

Figure 1.9. SEM images of PP nanocomposites containing (a) 1 wt.%, (b) 1.5 wt.%, and (c) 2.0 wt.% of GNs content from left to right [49].

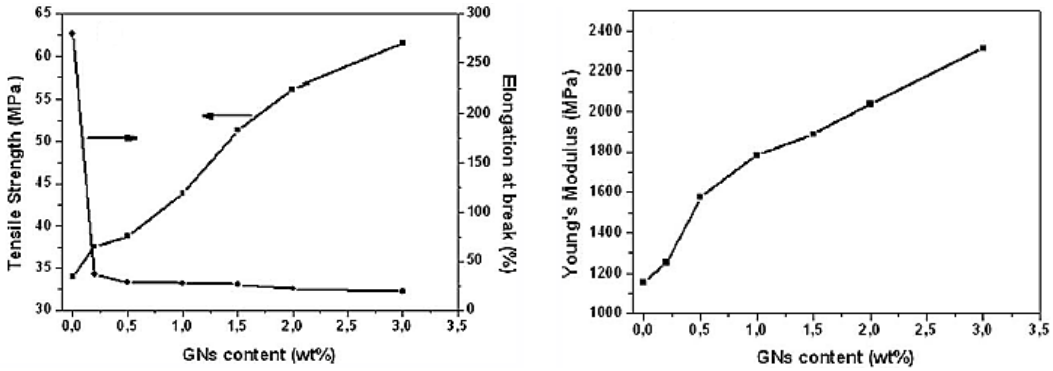

Figure 1.10. Tensile strength and modulus of elasticity curves with different GNs contents [49].

Based on the two-step manufacturing techniques, some researchers used intensive rolling and melt mixing techniques. Li *et al*. [50] found that using the two-step production method has increased the expanded graphite's degree of dispersion in the high density polyethylene resulting in the 15% tensile strength increase in the polystyrene (PS)/Expanded graphite masterbatch/HDPE and 22% increase in the polyethylene (PE)/EG masterbatch/HDPE. They also compared the nanoomposites produced in two-step with the direct melt blending and figured out that two-step process demonstrated much better performance than the single step method. Given the EG/PE and EG/PS masterbatches, they were both prepared by a two-roll mill, and then blended separetly with high density polyethelene by melt mixing. They also found that brittle fracture of the masterbatch nanocomposite confirming the excellent dispersion and exfoliation of expanded graphite layers in the matrices according to the SEM and X-ray tests, which had resulted in good mechanical properties.

Solid-state shear pulverization (SSSP) method was found by some researchers to have considerable contribution in increasing the mechanical characteristics of nanocomposites. Wakabayashi *et al*. [51] found that the solid state shear pulverization technique was an appropriate method in manufacturing as-received graphite based polymeric matrice nanocomposites. They compared the tensile test results of nanocomposites produced by SSSP with the ones obtained by the melt mixing process and observed the considerable property improvements with the graphite content at 2.5 wt.% resulting in a 100% increase in the tensile strength and a 60% increase in the elongation at break.

1.1.6.2. Unbalanced Behaviour of Mechanical Properties. In some studies, the tensile strength and modulus of elasticity demonstrated a complicated trend by increasing the amount of nanofiller loading. Mechanical properties of nanocomposites are enhanced up to the peak value at a critical fibre concentration, and then detoriorate with further fibre loading. Alternatively, at extremely low loading, the mechanical properties were decreased to some extent of nanofiller loading, then increased up to the peak value, and again decreased by further loading. There must have been many reasons behind the unstable mechanical performance such as ineffective dispersion at higher loading of nanofibers resulting in more stress concentration sites and weak interfacial interaction, agglomeration of nanofillers in the matrix preventing their mechanical properties to be transferred regularly to the matrix, and unevenly distribution of nanofillers in the matrix.

One of the studies, which have demonstrated this complicated trend -decrease, increase and then decrease- was the research carried out by Istrate *et al*. [52] who applied two step production method containing solution mixing using N-methyl-pyrrolidone solvent and melt mixing in order to manufacture exfoliated graphene nanoflakes reinforced polyethylene terephthalate. They observed that tensile strength and strain at break exhibit a similar trend as shown in Figure 1.11. The straightforward correlation between two mechanical properties corresponds to the formation of fibrillation. Exposed to tensile test at very low graphene content (0.03 wt.%), nanocomposites tended to form small fibrils illustrated in Figure 1.12. Since the graphene nanoflakes prevent the reorientation of the the polymer chains, this causes splitting of the material into molecular bundles and cavities leading to local failure and premature fracture resulting in finer fibrillation which has been the aspect of brittle fracture (low tensile strength is consistant with low strain at break). At relatively high graphene content (0.07 wt.%), however, larger fibrillations, corresponding to the semicrystalline area, were created shown in Figure 1.12 indicating an increase in both elongation at break and tensile strength.

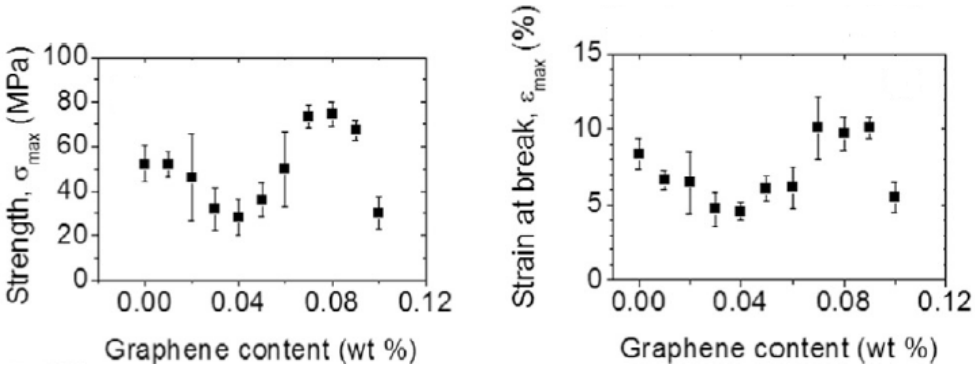

Figure 1.11. Tensile strength and elongation at break curves with different graphene contents [52].

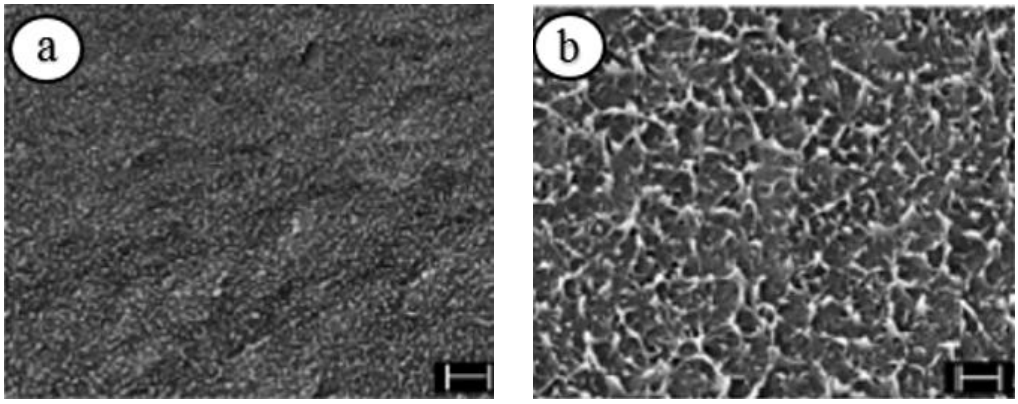

Figure 1.12. SEM images of: (a) PET/graphene nanocomposite (0.03 wt.%) and (b) PET/graphene nanocomposite (0.07 wt.%) [52].

In another study in which additional nanoparticle loading resulted in the decrease in tensile strength and modulus of elasiticity was the research done by Song *et al*. [53] who performed the production in two consecutive steps corresponding to the coating of GnPs with PP latex using in situ polymerization and melt mixing processes. They found that the coating of graphene nanoplatelets with polypropylene latex is the appropriate method to disperse the nanofillers in the polymer using melt mixing and solution mixing resulting in good mechanical properties with 63% increase in the tensile strength and 90% increase in the Young's modulus at maximum 0.5 wt.% graphene loading. However, mechanical properties of the nanocomposite started to decrease when the amount of nanofiller was increased. In fact, they found that this property change could be ascribed to plastization effect caused by the presence of low molecular PP latex due to its very low mechanical properties

in comparison to the polypropylene matrix. The x-ray diffraction results demonstrated complete exfoliation of graphene nanoplatelets in the polypropylene matrix.

1.1.7. Effect of Carbon Nanoparticles on a Polymeric Matrix in terms of Electrical Conductivities

Conductive Polymer Composites (CPCs) constituting of conductive fillers such as CNT, graphene, and CB, dispersed in a polymer matrices, draw attention from academic to industrial studies. They can be used in many industrial applications such as electrically conducting adhesives, antistatic coatings and films, electromagnetic interface shielding materials for electronic devices, thermal interface materials, etc. Generally, to obtain significant electrical conductivity of the order of 10^{-9} to 10^{-3} S/cm, polymeric systems need to have the substantial amount of conductive fillers. The most important concept in the field of electrically conductive composites is the percolation threshold in which the composites' characteristics translates from insulating to conducting. In fact, fillers in the polymeric systems strive to form a kind of network providing the balance between filler-polymer and filler-filler interactions, which ease the electrical conduction through the composites [54, 55]. Figure 1.13. illustrates a schematic of conductive path formation in a CPCs.

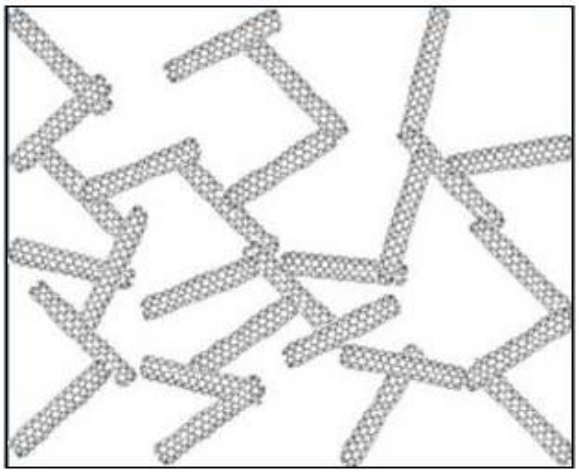

Figure 1.13. Schematic of conductive network formation in a CPC [55].

By manipulation of conductive network in CPCs, the wide range of conductivity can be presented in different stages staring from insulative to semiconductive and conductive materials. In fact, the level of conductivity deterimines the area of applications, which the CPCs are used [Figure 1.14., Table 1.1, 56, 57].

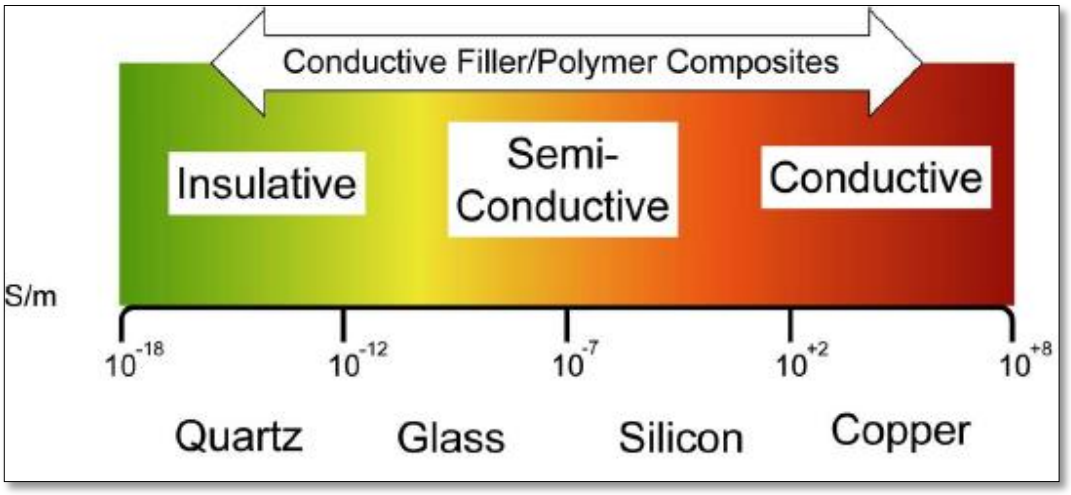

Figure 1.14. The approximate range of electrical conductivity covered by CPCs [56].

Table 1.1. CPC applications with their required range of electrical conductivity [57].

Application	Electrical Conductivity ($S.m^{-1}$)
Charge Storage	$<10^{-11}$
Antistatic Dissipation	10^{-7}-10^{-10}
ESD Protection	10^{-3}-10^{-6}
EMI Shielding	$>10^{+1}$

Electrical conductivity begins from the electric current (ordered movement of charges). The conduction electrons are dissipated freely in a solid due to their thermal energy in the absence of electric field. The force on an electron e is –eE and it is accelerated in the opposite direction to the electric field due to its negative charge if the electric field, E, has applied. So, there will be a net velocity, and the current density J can be calculated as indicated below where N_e is the number of electrons, e is the charge of electron, μ is the electron mobility, and E is the applied electric field [58]

$$J = N_e .\ e\ .\mu .E \tag{1.1}$$

Moreover, the applied electric field equals to the applied voltage over thickness of the sample. The electrical conductivity of the sample is defined as follows:

$$\sigma = \frac{J}{E} \tag{1.2}$$

Where σ is the electrical conductivity and its SI unit is S/m. Actually, the conductivity of insulators is usually less than 10^{-12} S/m, that of semi-conductors spans between 10^{-12} and 10^{+2} S/m, and finally for the conductors, it is more than 10^{+2} S/m. The materials' conductivitity can be elucidated using the Band Theory [59] in which the energy level of each electron can be deemed as a horizontal line. Since there are large numbers of electron in solids with various energy levels, the sets of energy levels generate two continuous energy bands, one of which is called the valence band and the other one is named as the conduction band. The energy gap between two bands demonstrates the prohibited region for electrons. Given the Band theory, elctrons constrained to individual atoms or interatomic bonds are involved in the Valence band while the others having enough energy to be delocalized by an applied electric field are said to be in the conduction band. For example, metals represent very high conductivity due to the overlap of two energy levels resulting in a good electron transformation between two bands. Further, although there is a gap between two energy levels in semiconductors, the gap is small enough so that electrons are excited by thermal energy and they are transferred from valence band to conduction band. Insulators, on the other hand, have the biggest gap between two bands, which restricts the electron transformation from one phase to another one resulting in a very low conductivity shown in figure 1.15.

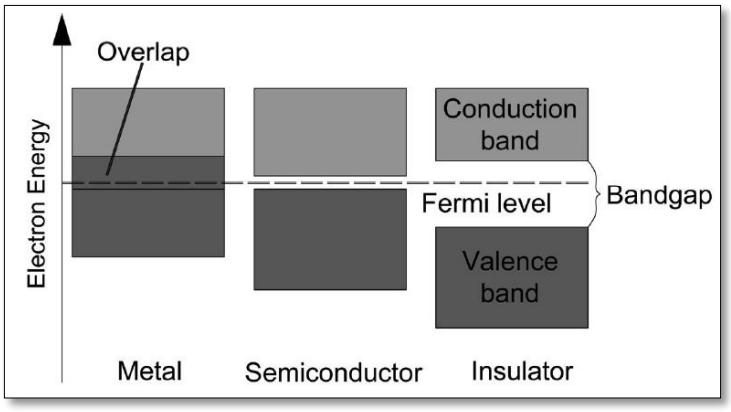

Figure 1.15. Simplified diagram of the electronic band structure in the Band theory [59].

Over the years, there has been a wide range of studies [60] aiming at better understanding the influence of different parameters on the percolation threshold of the carbon based polymer composites. In this respect, some of the important influencing factors are pointed out such as polarity of the polymer, degree of polymer crystallization, multiphase polymer matrices, viscosity of the polymer, fiber orientation, and types of conductive fillers. Therefore, the studies are divided into two sections; firstly, the effects of different parameters on the percolation threshold are reviewed, and secondly, the effects of manufacturing methods on the percolation threshold are taken into account.

1.1.7.1. The Effect of Different Parameters on the Electrical Percolation Threshold.
Miyasaka and co-workers [61] examined the effects of various types of polymer matrices on the conductivity of the composite with regard to the percolation threshold and found that polymers's polarity influences the amount of critical filler loading such that the higher the polarity, the more the filler content needed to be added to the matrix. They also figured out that the higher the surface tension of polymers, the larger the filler critical loading.

Sau *et al*. [62, 63] investigated the conductive rubber composites from various blends of ethylene-propylene-diene rubber and nitrile rubber and found that the percolation threshold is dependent on the viscosity of the polymers and concluded that the more the viscosity, the higher the percolation limit. In fact, if the viscosity of the base polymer is high, parameters in the blending method are changed such as feeding rate, temperature, rotation

speed which all together results in the degration of the carbon base fillers due to high shearing action. Therefore, the time to reach the percolation threshold is delayed due to the delay in the formation of the electrical network between carbon particles.

Nakis and Vaxman [64] studied the electrical resistivity of the conductive carbon based polyethylene composites and found that the threshold of semicrystalline materials is lower than the amorphous polymers. Gubblels et al. [65] found that the percolation threshold can be significantly reduced by the selective localization of carbon black particles in multiphase polymeric matrices.

Foulger *et al*. [66] found that the percolation threshold of the polymeric blends such as EVA/ (HDPE)/CB) can be achieved at much lower carbon filler content as compared with individually filled HDPE or EVA. There are two reasons: First, localization of the carbon black (CB) particles in the interface of two immiscible polymers leading to decrease of resistivity for the same CB percentage, and the other one can be the stress applied by the CB-rich area to the CB-poor polymer region, which also decrease the resisitivity.

Moreover, each of the carbonaceous fillers has intrinsic properties, which distinguish them. In this respect, Pramanik *et al*. [67] investigated different fillers on nitrile rubber and found that CB-fed polymer needed more fiber loading than CF-fed polymer. Furthermore, processing parameters, especially those containing considerable shear of polymer-fiber mixtures, have a great effect on the conductive properties of the final composite. So, it must be understood that the excellent mixing is the integration of homogenous dispersion of conductive fillers and good conduction improvements [63, 68, 69].

In one study, Zheng *et al*. [70] pointed out that the percolation threshold depends on the fibre orientation such that parallel fibres demonstareted the percolation threshold at about 3.65 vol.% CB loading whereas the perpendicular fibres illustrated its conductive point at 4.25 vol.% CB loading [Figure 1.16].

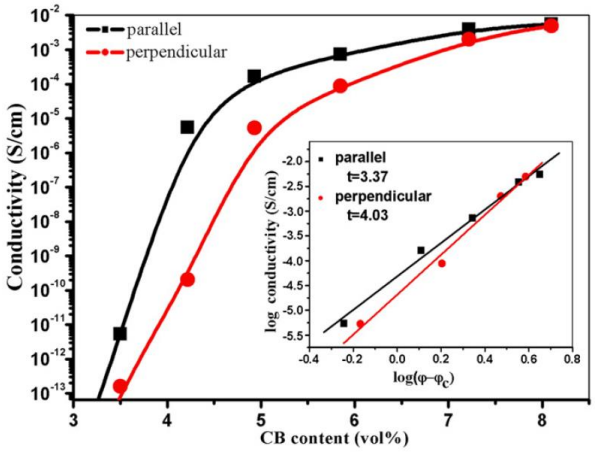

Figure 1.16. The electrical conductivity as a function of the CB content for the CPC samples in the parallel and perpendicular directions. The insert shows a log-log plot of the conductivity as a function of $\varphi - \varphi_c$ for the CPC [70].

1.1.7.2. Effect of production methods on the electrical percolation threshold. Different research studies were carried out to demonstrate the least possible percolation threshold which could be achieved. Among them, Hao-Bin Zhang *et al*. [71] examined the electrical conductivity of graphene reinforced polyethylene terephthalate nanocomposites using complete oxidation of graphite followed by thermal exfoliation and reduction. In this study, graphene nanosheets were prepared according to the work done by McAllister and coworkers [72]. Besides, GO was prepared through the Staudenmaier method [19] followed by blending with PET which resulted in superior electrical conductivity at a low percolation threshold of 0.47 vol.%. The high electrical conductivity of about 2.11 S/m was obtained only by adding 3.0 vol.% nanofiller loading content.

Kuvardina *et al*. [73] examined the effects of graphite nanoplatelets size on the mechanical, thermal, and electrical properties of exfoliated graphite based polypropylene nanocomposites. In this research, they took two kinds of xGnPs-(1&15) into consideration. To produce nanocomposite, polypropylene was first mixed with stabilizers of thermooxidative degradation in which there had been 0.3 wt.-% topanol and 0.5 wt.-% dilauriltiodipropionate. Then, xGnPs were slowly added to the PP at the loading range 0.5-10 vol.% (1-20 wt.%) using melt blending technique, and found that instead of improvement

in the mechanical and thermal properties of the nanocomposite, the electrical conductivity had also been achieved with the lowest percolation threshold at about 4 vol.%. [Figure 1.17].

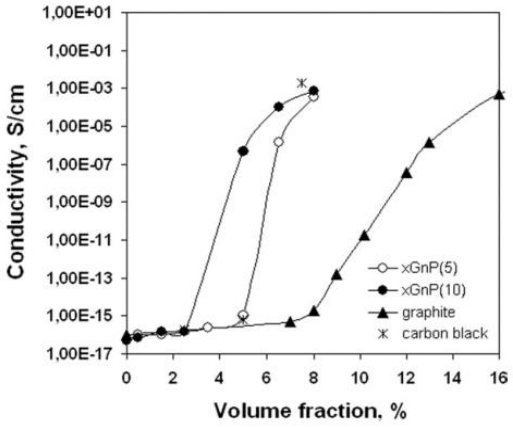

Figure 1.17. Conductivity of the PP composites with different types of fillers versus filler loading [73].

Furthermore, Verdejo *et al.* [74] did a review on the graphene filled nanocomposites. In this context, on-going advances on the production processes, their resultant properties, and also potential application were discussed. Reduced and unreduced GO were the most prioritized concepts in this research. Given the electrical conductivity, different polymer matrices, mixed with graphene, illustrated various percolation thresholds. Even though the electrical conductivity of the chemically modified graphene sheets was not as high as that of perfect graphene, it was still ideal candidate to achieve electrically conductive nanocomposites. In this context, low percolation thresholds were obtained with chemically reduced GO using hydrazine and isocyanate through solvent mixing while the largest one was achieved by the thermally exfoliated GO via melt blending [Figure 1.18].

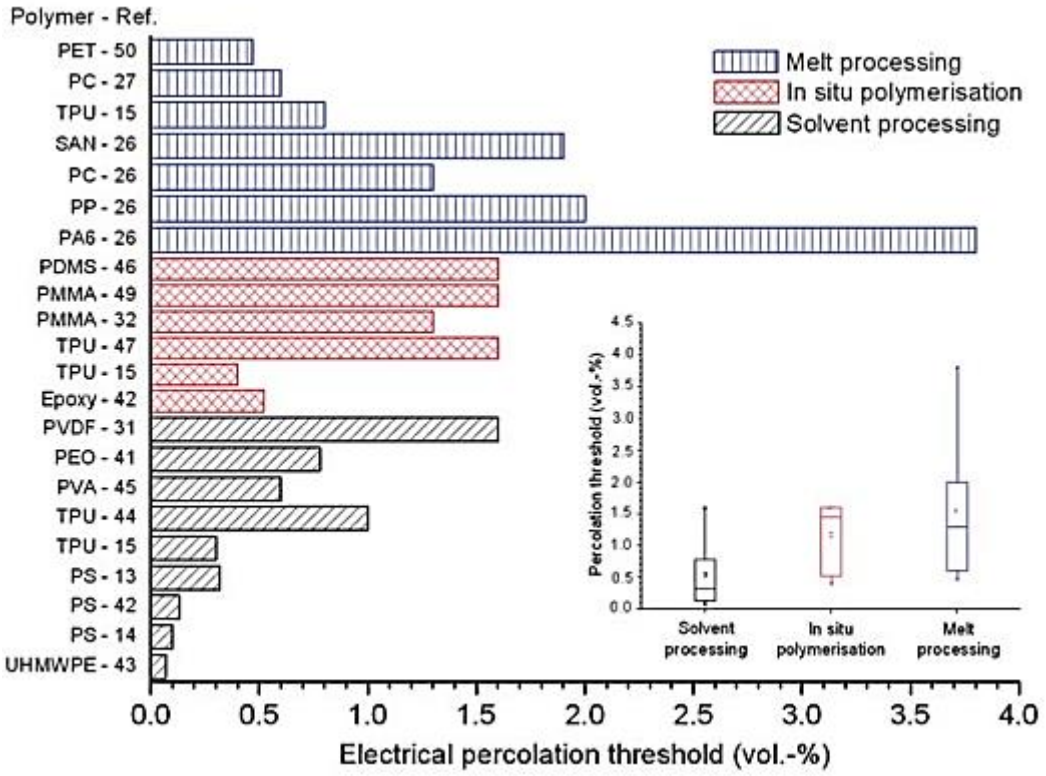

Figure 1.18. Electrical percolation thresholds of graphene/polymer nanocomposites according to processing strategy [74].

Garzon *et al.* [75] prepared different kinds of nanofillers such as graphite, thermally reduced graphite, carbon nanotubes mixed with PP, and the effects of particles` type as well as the annealing process on the electrical behavior was analyzed. In this context, thermally reduced graphite oxide was achieved in two consecutive steps: First, graphite flakes were synthesized via hummers` method [20] to obtain graphite oxide; second, produced graphite oxide sheets were rapidly heated up to 600℃ to achieve TrGO. It should be noted that thermal shock was needed to exfoliate graphene sheets. Furthermore, to prepare nanofiller reinforced PP nanocomposite, melt mixing method was used with the filler loading between 0 and 12.5 vol.-% for TrGO or CNT, and 0 and 25 vol.-% for graphite. As with hybrid nanofillers, the polymer was added to the mixture, containing half of the polymer blended with an antioxidant, followed by the proper concentration of TrGO (1-2 vol.-%) along with CNT (0-2 vol.-%). Consequently, carbon based filler aspect ratio had a great impact on the electrical conductivity of the nanocomposites. In fact, alligned CNTs and TrGO could have a low percolation threshold with small amount of concentration. Moreover, annealing effects

on the graphite/PP, and CNT/PP demonstrated relevant increase in the electrical conductivity. Nevertheless, annealing process did not show any variations on the conductivity of TrGO/PP. Also, it was worthwhile mentioning that the addition of second nanofiller like CNTs to the TrGO/PP nanocomposites resulted in the electrical conductivity increase. [Figure 1.19 & Figure 1.20]

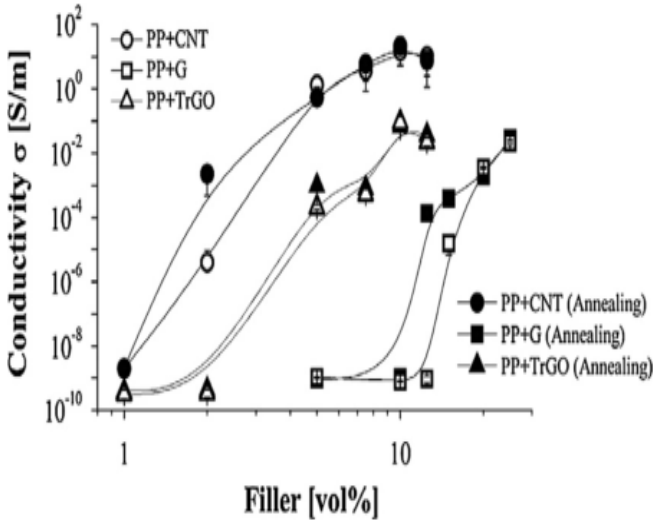

Figure 1.19. Effect of carbon based fillers and annealing (30 min at 190℃) on the electrical conductivity of PP composites [75].

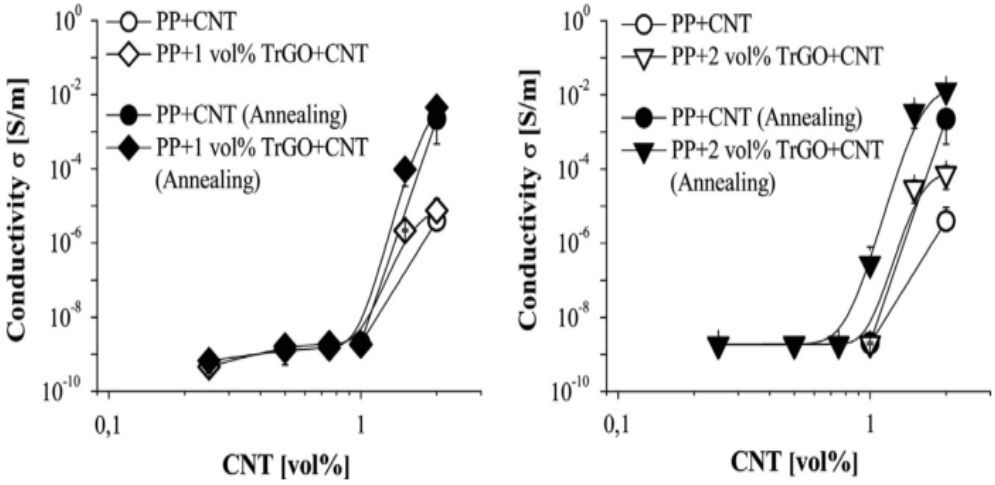

Figure 1.20. Effect of CNT and annealing (30 min at 190℃) on the electrical conductivity of PP/TrGO/CNT hybrid composites. Hybrid composites with 1.0 vol.-% of TrGO (left) and hybrid composites with 2.0 vol.-% of TrGO (right) [75].

Finally, Li *et al*. [76] reviewed the effect of various production methods on the electrical percolation threshold and found that polymer/GNPs nanocomposites produced by "wet" methods, such as in situ polymerization and solution mixing with the help of ultrasonication, often have the low electrical percolation threshold in comparison with other fabrication methods. For example, masterbatch filling, melt compounding, and solution mixing (master batch) plus injection molding are among the methods which have demonstrated higher percolation threshold compared to wet methods. However, they pointed out that the coating technique could be an appropriate method in increasing the exfoliation and dispersion of graphene nanoplatelets in the polymeric matrices. Therefore, the effects of production methods on the electrical percolation threshold of the nanocomposites were summarized in Table 1.2.

Table 1.2. Electrical properties of polymer/GNP nanocomposites.

Polymer	Dimensions of GNP (d diameter, t thickness)	Pretreatment/ fabrication of GNP	Fabrication of nanocomposites	Percolation threshold	Electrical condusctivity (S/cm)
PP	1 μm (d) 10 nm (t)	-	Coating + compression molding	0.1 vol.%	$\sim10^{-4}$ at 3.0 vol.%
HDPE	5 μm (d) 70 nm (t)	-	Melt mixing	2.53 vol.%	$\sim10^{-6}$ at 8.0 wt.%
HDPE	N/A	-	Master batch filling technique	16.0 wt.%	$\sim10^{-4}$ at 25.0 wt.%
HDPE	N/A	Modified by unsaturated polyster resin	Melt mixing	5.7 wt.%	$\sim10^{-4}$ at 8.0 wt.%
Epoxy	N/A	UV/ozone treatment	Curing + ultrasonication	N/A	$\sim10^{-5}$ at 2.0 wt.%
		-			$\sim10^{-6}$ at 2.0 wt.%
Epoxy	5-10 μm (d) 10-100 nm (t)	Nitric acid treatment	Curing + ultrasonication	< 0.5 vol.%	$\sim10^{-4}$ at 4.0 vol.%
		-		<2 vol.%	

Table 1.2. Electrical properties of polymer/GNP nanocomposites (Cont.)

Polymer	Dimensions of GNP (d diameter, t thickness)	Pretreatment/ fabrication of GNP	Fabrication of nanocomposites	Percolation threshold	Electrical condusctivity (S/cm)
Epoxy	N/A	Bromination	Curing + ultrasonication	1 wt.%	$\sim 10^{-4}$ at 2.0 wt.%
PVDF	10 μm (d) 50 nm (t)	-	Solution casting + ultrasonication	2.4 wt.%	$\sim 10^{-4}$ at 4.0 wt.%
PVA	N/A	Electrochemically modified	Solution casting + ultrasonication	6.0 wt.%	$\sim 10^{-7}$ at 7.0 wt.%
CMPVA	N/A	-	Solution casting + ultrasonication	0.8 wt.%	$\sim 10^{-6}$ at 4.0 wt.%
PMMA	10 nm (t)	-	Solution casting + precipitation	N/A	$\sim 10^{-4}$ at 5.0 wt.%
PMMA	N/A	Heating graphite oxide at 500°C for 20 min under N_2	In situ polymerization in the pores of GNPs	N/A	~60 at 8.0 wt.%
PMMA	N/A	Graphite oxide	In situ polymerization	~ 2.0 wt.%	$\sim 10^{-4}$ at 8.0 wt.%

Table 1.2. Electrical properties of polymer/GNP nanocomposites (Cont.)

Polymer	Dimensions of GNP (d diameter, t thickness)	Pretreatment/ fabrication of GNP	Fabrication of nanocomposites	Percolation threshold	Electrical condusctivity (S/cm)
LLDPE	15 μm (d) 10 nm (t)	Paraffin coating	Solution mixing (master batch) + melt compounding	N/A	~10^{-4}
LLDPE	15 μm (d) 5-10 nm (t)	Microwave radiation	Solution mixing (master batch) + injection molding	12-15 wt.%	~10^{-7} at 20.0 wt.%
Acrylonitrile styrene copolymer	N/A	-	Master batch filling technique	9.0 wt.%	~10^{-3} at 15.0 wt.%
PLA	N/A	-	Melt mixing	3-5 wt.%	~10^{-7} at 7.0 wt.%
Cojugated PAN	46 μm (d) 4.5 nm (t)	-	Solution casting + ultrasonication	3-4 wt.%	~10^{-3} at 6.0 wt.%
PEN	485 nm (d) 36 nm (t)	Graphite oxide	Melt compounding	0.3 vol.% (Surface resistance)	-
TPV (PE/EPDM)	N/A	PP-g-MA/ GNP master batch	Melt compounding	6 phr	~10^{-4} at 15.0 wt.%
PS	5-10 μm (d) 80-150 nm (t)	-	In situ polymerization	0.011 vol.%	~10^{-3} at 0.03 vol.%

Table 1.2. Electrical properties of polymer/GNP nanocomposites (Cont.)

Polymer	Dimensions of GNP (d diameter, t thickness)	Pretreatment/ fabrication of GNP	Fabrication of nanocomposites	Percolation threshold	Electrical condusctivity (S/cm)
Unsaturated polyester resin	N/A	-	In situ polymerization + ultrasonication	0.64 vol.%	-
Nylon-6	13.5 μm (d) 515 nm (t)	-	In situ polymerization + ultrasonication	0.75 vol.%	$\sim 10^{-3}$ at 3.0 wt.%
PODBS	> 500 nm (d) 10-40 nm (t)	Microwave radiation followed by ultrasonication	In situ melt polymerization	4.0 wt.%	$\sim 10^{-3}$ at 5.0 wt.%
PANI	0.5 μm (d) 30-100 nm (t)	Microwave radiation followed by ultrasonication	In situ polymerization	1.5 wt.%	~33.3 at 1.3 wt.%
Silicone rubber	0.5-20 μm (d) 30-80 nm (t)	-	Wet mixing + curing	0.9 vol.%	$\sim 10^{-5}$ at 2.0 vol.%

1.2. Problem Statement

Despite the fact that there have been so many studies in the field of nanocomposites, there is still difficulty in optimizing the process parameters. Besides, industrial applications of these materials are the matter of importance since it must be economical. Therefore, researchers working on nanocomposites are both presenting different production techniques which would yield cost-effective and high quality nanocomposites and would improve the process parameters such as temperature, mixing time, pressure, feeding rate, rotation speed, as well as compatibility between fibre and polymer, and stability of the suspensions (Graphene platelets suspended in different solutions and ready to be transferred to the base polymer).

Before Graphene was invented, the great deal of studies was carried on using CNTs and CB. In spite of the fact that CNTs were proved to have high mechanical, electrical and thermal conductivity due to its high aspect ratio and surface area compared to CBs that could accelerate the formation of percolation network, its agglomeration after being produced in a reactor along with the limitation to the fibre loading are making the process difficult. Besides, CNTs tend to buckle quickly when they undergo compressive, torsional, and bending stresses due to their hollow structures [77-80]. Moreover, CBs tend to form the percolation network with high CB loading due to its small surface area in comparison with Graphene and CNTs, and this fact could negatively affect other material properties and increase the final product cost simultaneously [81]. Graphene invention in 2004 marked a major turning point in the material science that provided the balance between cost and processability. Therefore, to mention some of the properties that distinguish graphene from its counterparts, the characteristics have already been recorded and illustrated in Table 1.3 [82-84].

Table 1.3. Properties of single layer graphene [85].

Young`s modulus	1 TPa
Tensile strength	130 GPa
Thermal conductivity	5000 W/m°k
Surface area	2630 m^2/g
Carrier mobility	200000 cm2/vs
Transparency	97.7 %

The first priority of the current study is improving the electrical conductivity of polypropylene to obtain a low cost, highly conductive carbon nanoparticle based nanocomposites with relatively easy processing at mass scale without jeopardising the mechanical properties. In this respect, most of the aforementioned studies are focused on mixing the functionalized carbon nanoparticles with the polymeric matrix. However in this study, the major objective is to produce electrically conductive polymers without any degradation in mechanical properties. So, graphene nanoplatelets are used as received without any functionalization. Dispersion is prioritized rather than particles functionalization. Furthermre, this was the first time that graphene based nanocomposite research was carried out at Bogaziçi University Composites Laboratory. Therefore, Graphene suspensions are prepared using a proper surfactant, suspended in water, blended with the polypropylene through the melt mixing process and the electrical and mechanical properties of the resulting nanocomposite were compared to carbon black-polypropylene nanocomposites at different CB weight fractions.

2. EXPERIMENTAL WORK

During this study, several carbon particle based polymeric composites and nanocomposites were manufactured. First, micro-scale short carbon fibre based PA6 and PP composites were manufactured by melt mixing in a twin screw extruder. Secondly, CB based polypropylene with different weight fractions were manufactured by diluting a commercially available CB/PP masterbatch of 40 wt% CB with neat PP in the twin screw extruder. Finally, exfoliated graphene nanoplatelets based polypropylene (xGnPs-PP) nanocomposites was produced by first preparing stable suspensions of graphene nanoplatelets in water with the help of a proper surfactant and then liquid feeding this suspension to molten PP in a twin screw extruder and melt mixing. Then rheological, mechanical and electrical properties of the nanocomposites are explored.

2.1. Materials and Manufacturing

2.1.1. Materials

As indicated, various kinds of materials used as filler or as matrix were obtained from different companies. PA6 is supplied by DuPont with a tradename of Zytel® FE210021 NC010. Maleic Anhydrate grafted Polypropylene (MA-g-PP) specified as PP4 were provided by Polyone. PP is supplied by Lyondellbasell with a trademark of Moplen® HP500N. Carbon fibres compatible with PP are received from DowAksa with the product number of CCF141001001. Carbon black (type N220)–Polypropylene masterbatch compatible with PP is received from Aksoy Plastik from with the product code as PP/E 19844. Finally, industrial graphene nanoplatelets for general purpose were provided by Grafen Co. with the thickness between 5-10 nm, diameter between 5-10 μm, purity <99%.

Besides, in defing the graphene characteristics, Raman Spectroscopy along with SEM images were presented in the data sheet and shown in Figure 2.1, and Figure 2.2 [81, 86]. In fact, Raman spectroscopy is employed to understand the spectrum of pure PP, GnPs, and

GnPs/PP composites such as the presence of defects, stacking order, and the state of oxidation. For example, specific to graphene nanoplatelets, three important recorded peaks are D, G, and 2D bands. The D band value, known as defect band, and it is very weak, is located at ~ 1338 cm^{-1}. Actually, the primary formation of graphene and graphite is the G band, which is normally located at ~1585 cm^{-1}. Finally, the 2D band demonstrates the stacking layers of graphene, which is created at ~2750 cm^{-1}.

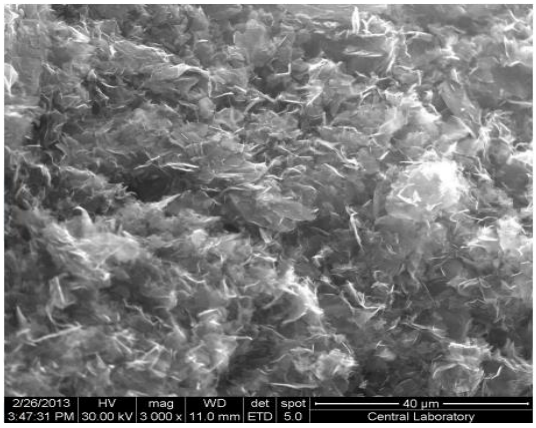

Figure 2.1. Scanning Electron Microscopy of Graphene nanoplatelets [86].

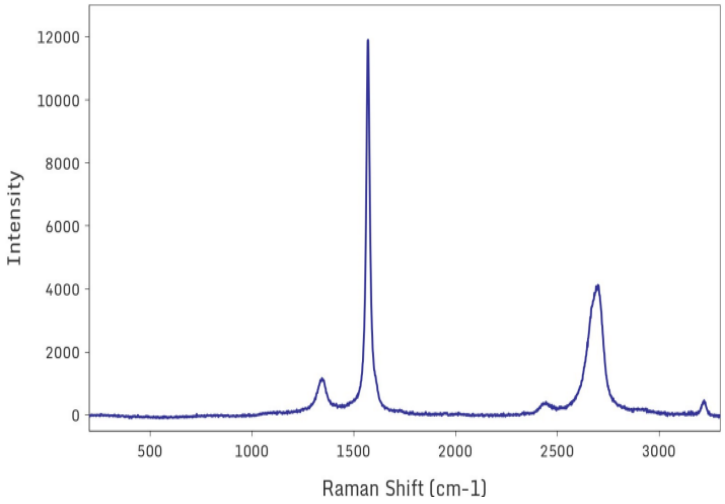

Figure 2.2. Raman spectroscopy-Graphene nanoplatelets [86].

2.1.2. Equipment

The twin screw extruder, assembled by Gulnar Plastic Company, has configurable screws having an L/D ratio of 44, a barrel diameter of 12 mm, two gravimetric feeders for plastics and minerals and fibres, one volumetric feeder for feeding fluids. The extruder can

operate at temperatures up to 400° C and is used to mix two different material phases using two different screw set-ups prepared for composites and nanocomposites. These screw sep-ups were illustrated below in Figure 2.3, and Figure 2.4 [87]. Further, an injection-molding machine Arburg Allrounder 275V, was used to produce the dog-bone shaped composite and nanocomposite tensile samples for further evaluations. The specifications of the injection molding machine was as follows: clamping force of 250 kN, injector stroke of 60 mm, enjector force of 20 kN, Screw diameter of 25 mm, maximum injection volume of 49 cm^3, and maximum injection pressure 2000 bar. Moreover, to prepare the nanofluids solution, Hielscher Ultrasonic Dispenser with 1000 W adjustable power with the 1.5 lt recirculating reservoir was used. A vacuum oven manufactured by Nüve with model number of EV 018 and the maxiumum temperature of 200 °C was used to dry the samples.

2.2. Specimen Preparation

Carbon Fibre-Polypropylene (CF-PP) and Carbon Fibre-Polyamide (CF-PA6) composites were manufactured in two steps: In the first step, the carbon fibres and polymers were placed in the oven with the vaccum to be completely dried to prevent any defects such as bubbles in the final composite. In the second step, fibre and polymer is compounded through the melt mixing technique.

Carbon Black-Polypropylene (CB-PP) nanocomposites were manufactured by diluting the PP masterbatch with 40 wt% CB in the twin screw extruder. The PP-CB masterbatch is fed to the twin screw extruder through the main feeder whereas neat PP is fed through the side feeder.

Expanded Graphene Nanoplatelets-Polypropylene (xGnPs-PP) nanocomposites, on the other hand, were processed in three steps: In the first step, as-received graphene nanoplatelets in the form of powder were mechanically shear mixed with the sodium dodecyl sulfate (SDS) as a surfactant in the water. In the second step, the mixture is processed by ultrasonication in order to have a suspension that can stay stable for a certain period of time to be fed into the extruder without precipitation. After the nanofluid suspension was prepared, the third step is then feeding the nanofluid suspension into the molten PP in the

extruder. The processing temperature of the molten polymer enables evaporation of the water from the suspension and to be removed from the vacuum port. Process parameters are optimized to obtain homogenously distributed and dispersed composites and nanocomposites with the appropriate viscosity. Some of these important parameters were temperature range, feeding zone depending on the screws configuration, feeding rate, and rotation speed of the shafts. So, the extrusion related parameters were unique for each material and trial and error technique was the only procedure that had been used in this research to obtain the optimum parameters. In other words, to be able to pelletize the final product coming out of the extruder's die, its viscosity had been visually and practically examined to be sure that either the nanocomposite strands are viscous enough to be pulled through the cooling water without loosing their integrity. To do that, the materials' rheological characteristics such as melting point, degree of crystallization, and degradation point were carefully assessed, then the parameters were optimized accordingly. First, the temperature profile was set according to the rheological values of the polymeric matrix provided by the supplier such that it began with its lowest temperature in the first zone and reached to its maximum in the last zone. Also, the melting temperature defined for the polymer by the supplier was set to be the start of melting and mixing zone temperature, and then it was increased from one zone to the next. Second, the shafts rotation speed was specified by taking into account the output product's viscosity and throughput. Finally, after melt compounding composites or nanocomposites in twin screw extruder, they are pelletized in the form of granules, and were injection molded and the dog-bone shaped tensile test samples were produced.

2.2.1. Carbon Fibre-Polyamide (CF-PA6) and Carbon Fibre-Polypropylene (CF-PP) Composites

PA6 granules were vacuum dried for about 120 min at 70℃. Also, carbon fibre was vacuum dried for about 120 min at 85℃. After that, PA6 was placed in the extruder's main hopper whereas the chopped CFs were put into its side feeder with gravimetric ratio of 90 wt% PA6 to 10 wt% CF. After the desired temperature profile was obtained, the extrusion compounding process with an appropriate screw configuration was run. Having reached the desired amount of composite viscosity, the composite strings were pulled along the 20℃ to 30℃ water bath in order to be solidified and pelletized. Then, the pellets were vacuum dried

in the oven at 94℃ for 120 min. The dried pellets were then processed by the injection molding machine to produce the dog-bone shaped tensile test samples for further analyses.

Screw configuration suitable for composites have three important zones: (i) intake or solid conveying zone, (ii) melting and mixing zones, (iii) the metering zone in which the compounded polymer melt was transferred to the die by drag flow caused by the rotating action of the screws. To create indicated zones, the function of different types of screws had to be well understood. So, the schematic drawing of the twin-screw compounding extruder, screw configuration and barrel temperature profiles for the twin screw extruder were shown at Figures 2.3, 2.4, 2.5, and 2.6.

The process parameters were optimized such as temperature profile, shafts' rotational speed, feeding rate, injection pressure, holding pressure, and holding time. All of the process parameters for both extrusion and injection molding processes were shown in figures 2.8 and 2.9, and summarized in Tables 2.1 and 2.2. The reason that the parameters were changed from one experiment to another was due to the different characteristics of molten composite along with fibre weight fractions in the matrix. Screw configuration, on the other hand, was an important factor in obtaing good dispersion and distribution of the fibres in the matrix.

Generally, given the extrusion processes, to achieve an appropriate product viscosity and steady and stable process, all of the aforementioned process parameters were optimized. Temperature profile depending on the matrix melting point were set up, then depending on the type of filler added, all other interdependent parameters were arranged although temperature profile was sometimes subjected to change to obtain an acceptable viscosity.

The schematic of the injection molding process is shown in Figure 2.7. As for parameters of the injection molding process, injection pressure could not be too low since it would produce a short shot, and also it could not be too high since it would flash the mold. Moreover, holding pressure applied to compensate for material shrinkage was found to be approximately 50% of the injection pressure would to have satisfactory products with minimum shrinkage. Besides, holding time while applying the holding pressure was kept constant for all experiments.

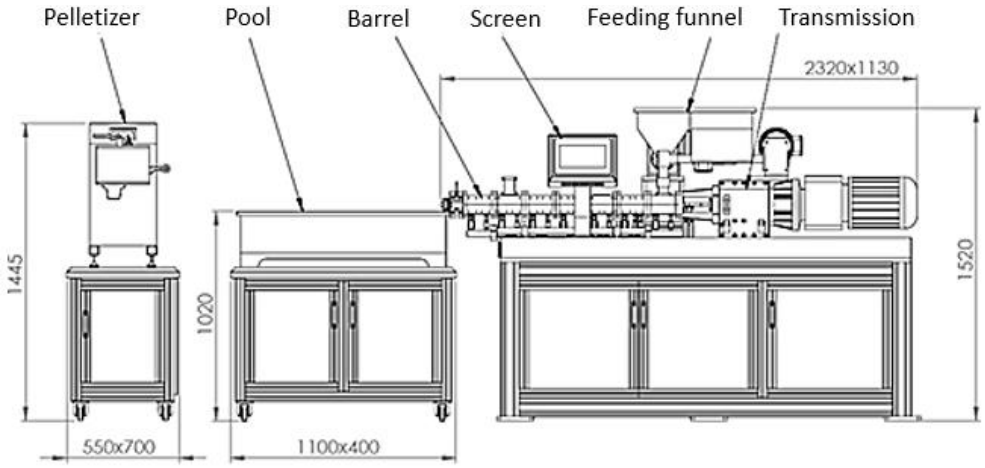

Figure 2.3. The schematic of the twin-screw compounding extruder.

Figure 2.4. Types of modular screws assembled on high torque splined shafts (conveying element, melting and mixing elements, intake element from left to right) [87].

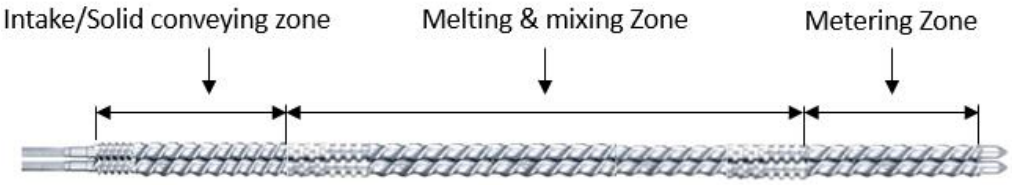

Figure 2.5. Screws configuration for CF based PP and CF based PA6 composites [87].

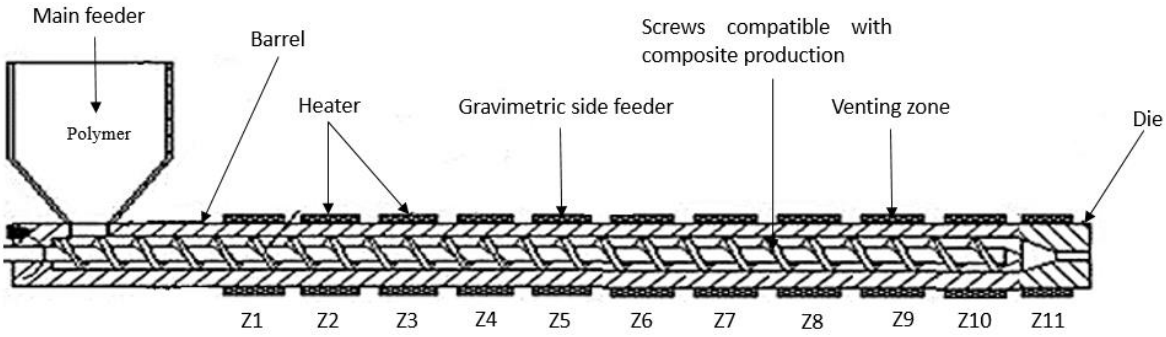

Figure 2.6. Schematic of the screw configuration and extruder configuration for compounding CF-polymer composites. For temperature profile, refer to Table 2.1.

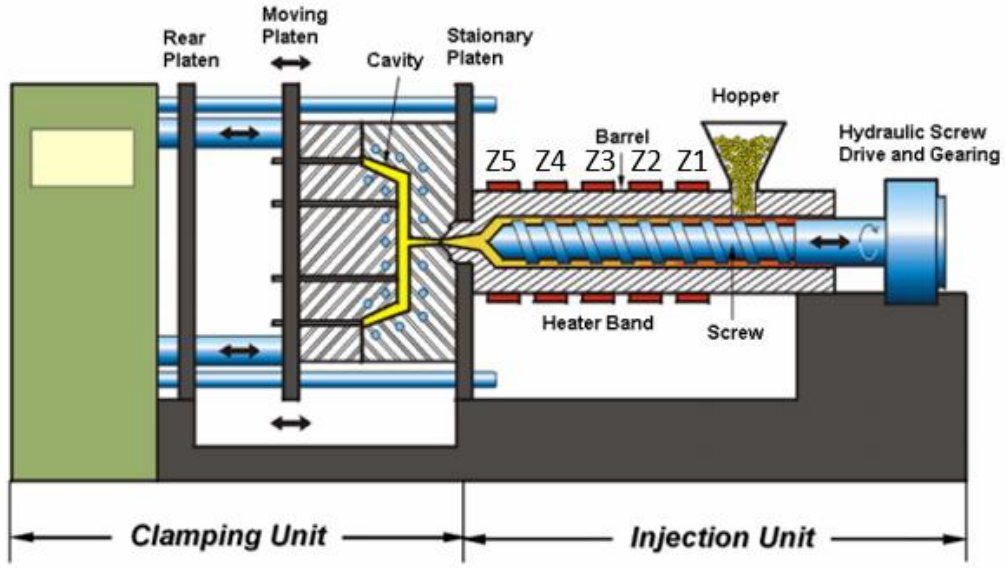

Figure 2.7. The schematic drawing of a typical injection molding machine.

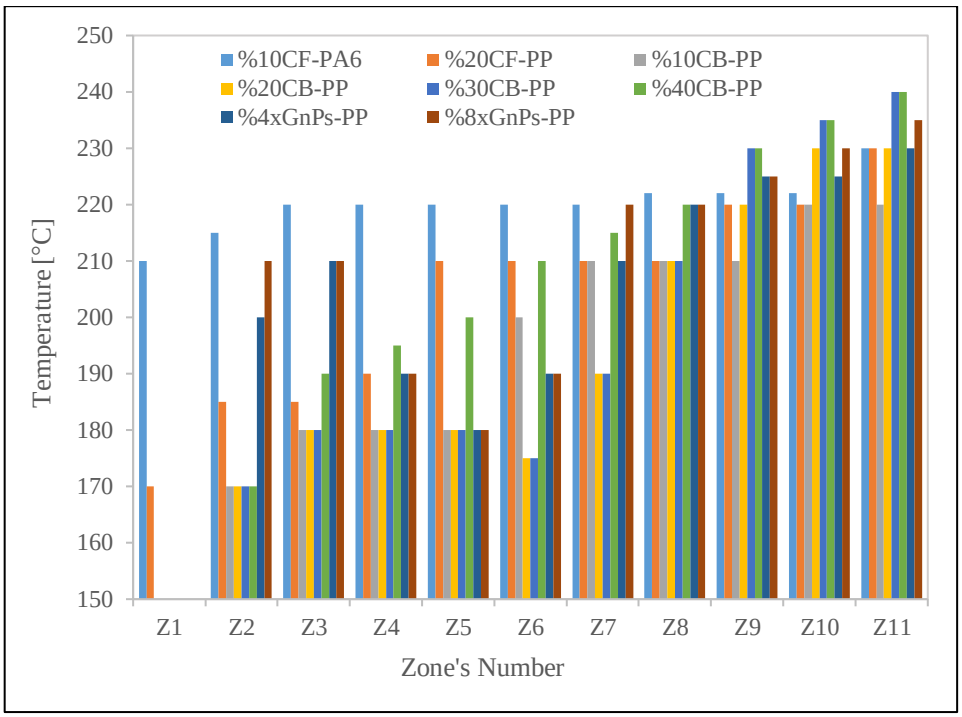

Figure 2.8. Melt blending temperature profile per each zone with respect to nanofillers loading.

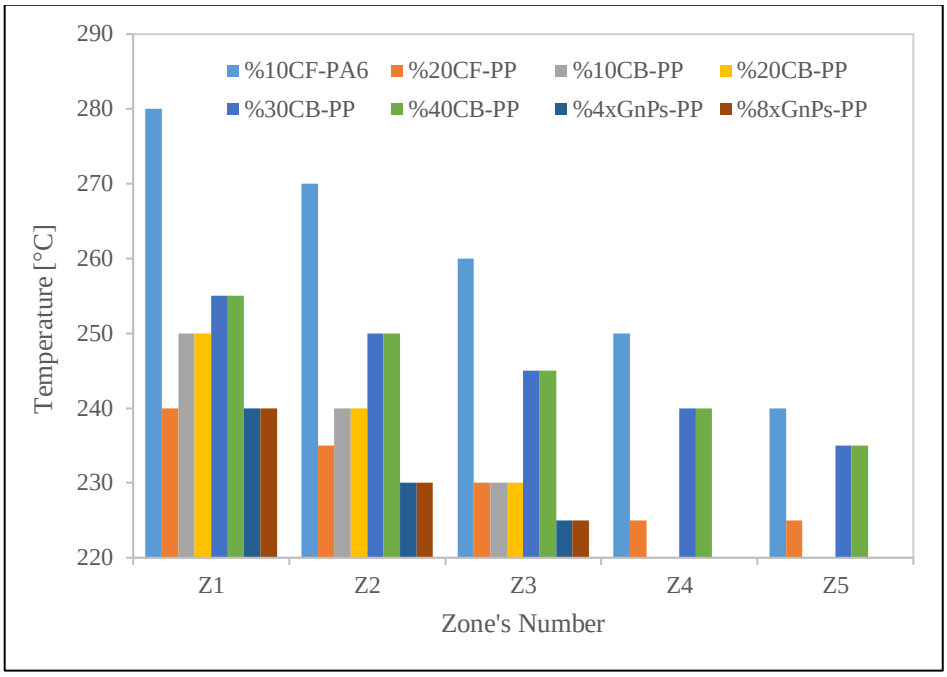

Figure 2.9. Injection molding temperature profile per each zone with respect to nanofillers loading.

Table 2.1. Temperature profiles- Extrusion and injection molding process.

Extrusion-Temperature profile											
Material/Zone	Z1 (°C) (Hopper)	Z2 (°C)	Z3 (°C)	Z4 (°C)	Z5 (°C)	Z6 (°C)	Z7 (°C)	Z8 (°C)	Z9 (°C)	Z10 (°C)	Z11(°C) (Die)
%10CF-PA6	210	215	220	220	220	220	220	222	222	222	230
%20CF-PP	170	185	185	190	210	210	210	210	220	220	230
%40CB-PP	150	170	190	195	200	210	215	220	230	235	240
%30CB-PP	150	170	180	180	180	175	190	210	230	235	240
%20CB-PP	150	170	180	180	180	175	190	210	220	230	230
%10CB-PP	150	170	180	180	180	200	210	210	210	220	220
%4xGnPs-PP	150	200	210	190	180	190	210	220	225	225	230
%8xGnPs-PP	150	210	210	190	180	190	220	220	225	230	235

Table 2.1. Temperature profiles- Extrusion and injection molding process (Cont.)

Material/Zone	Z1 (Hopper)	Z2	Z3	Z4	Z5 (Nozzle)	-	-	-	-
%10CF-PA6	280	270	260	250	240	-	-	-	-
%20CF-PP	240	235	230	225	225	-	-	-	-
%40CB-PP	255	250	245	240	235	-	-	-	-
%30CB-PP	255	250	245	240	235	-	-	-	-
%20CB-PP	250	240	230	220	220	-	-	-	-
%10CB-PP	250	240	230	220	220	-	-	-	-
%4xGnPs-PP	240	230	225	220	220	-	-	-	-
%8xGnPs-PP	240	230	225	220	220	-	-	-	-

Table 2.2. Process parameters- Extrusion and injection molding.

	Material	Main shafts speed (rpm)	Side Shafts speed (rpm)	Side feeder's feeding rate (gr/h)	Main feeder's feeding rate (gr/h)
Extrusion	%10CF-PA6	100	30	160	1600
	%20CF-PP	300	30	240	960
	%40CB-PP	240	-	-	400
	%30CB-PP	230	80	100	300
	%20CB-PP	220	80	150	150
	%10CB-PP	210	80	300	100
	%4xGnPs-PP	220	42	12	288
	%8xGnPs-PP	235	55	16	184

Table 2.2. Process parameters- Extrusion and injection molding (Cont.)

	Material	Injection pressure (bar)	Holding Pressure (bar)	Holding Time (s)	Volume (cm^3)
Injection molding	%10CF-PA6	1500	600	7	37
	%20CF-PP	1500	670	7	37
	%40CB-PP	1300	700	7	37
	%30CB-PP	1300	700	7	37
	%20CB-PP	1300	650	7	37
	%10CB-PP	1300	650	7	37
	%4xGnPs-PP	1300	650	7	37
	%8xGnPs-PP	1300	650	7	37

Moreover, as for the micro-scale Carbon Fibre-Polypropylene (CF-PP) composites with the presence of MA-g-PP as a compatibilizer, PP granules and compatibizers were mixed manually with the weight fraction of compatibilizer to polymer to be 2%, and then the mixture is vacuum dried in the oven at 70℃ for 120 min. Similarly, CFs were vacuum dried at 85℃ for 120 min. Then they were all undergone the compounding process such that the mixture of PP and compatibilizer were fed through the main feeder while the CFs were fed to the polymeric matrix through the side feeder. The screw has the same configuration applied to %10CF-PA6 composites. After composite strings with good processability conditions were produced and pelletized, and then the pellets were vacuum dried and put into the injection molding process. Details regarding the process parameters were indicated in Tables 2.1 and 2.2.

2.2.2. Production of Carbon Black-Polypropylene (CB-PP) nanocomposites

CB-PP nanocomposites were produced by reducing the weight fraction of 40% CB based PP masterbatch by melt mixing with neat PP to dilute the masterbatch. The screw configuration, shown at figure 2.10 and figure 2.11, were used for producing the CB-PP nanocomposites. Besides, other process parameters were also illustrated at Table 2.1 and Table 2.2. Screw configuration, assembled on the shafts, was different from the one used for producing the CF-composites since the structure of the nanocomposites did require more

shear mixing to disperse and distribute the nanoparticles uniformly in the polymeric matrix. The mixing operation was divided into two parts to be better understood: (i) dispersive mixing was defined as an exertion of shear stresses and longitudinal forces on the large agglomerated particles in the melt polymer by detaching individual units, (ii) distributive mixing, on the other hand, was described as a homogenous spatial rearrangement of particles in the base polymer matrix. In this respect, shafts, used for all compounding nanocomposites (CB-PP and xGnPs-PP nanocomposites), were designed to have six regions as shown in Figure 2.9: 1) intake and solid conveying segments, 2) melting region, 3) mixing zone, 4) melt conveying zone, 5) devolatization zone, and 6) metering region- to guarantee the quality of the final product. Meanwhile, devolatization segment was for eliminating any undesired volatile materials, and the metering region was for transferring the molten nanocomposite to the die by the assistance of conveying elements. In fact, devolatization zone was the combination of different elements such as mixing, conveying, back pressure elements and also the venting element. Before beginning the process, the masterbatch granules were vacuum dried at 90 ℃ for 120 min.

The injection molding parameters for each CB-PP nanocomposite are slightly varied according to the CB content, since the weight ratio of the CB significantly alters the viscosity and melt flow index of the nanocomposite. The process parameters were indicated at Tables 2.1 and 2.2. Moreover, the position of main feeder, the sider feeder, venting location, and screws are schematically as similar as the one set for composites shown in figure 2.6. For 30 and 20%CB-PP nanocomposites, the masterbatch was fed through the main feeder, and PP is fed through the side feeder, wheras for 10%CB-PP nanocomposite, the masterbatch is fed through the side feeder, and PP is fed through the main feeder.

Figure 2.10. Types of modular screws assembled on high torque splined shafts (Conveying element, mixing element, melting and mixing elements, intake element, and back pressure element from left to right).

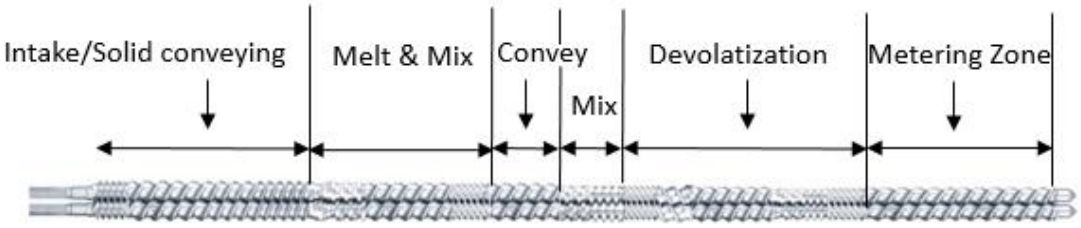

Figure 2.11. Screws configuration for CB based PP nanocomposites.

2.2.3. Production of Exfoliated Graphene Nanoplatelets-Polypropylene (xGnPs-PP) nanocomposites

Since the graphene nanoplatelets were achieved in the form of powder, they would not be easily injected to the polymer as such, so they had to be suspended in the liquidus material such as water. However, it was observed that graphene nanoplatelets on its own could not be stable in the water and agglomerates once the mixing process was completed. Three different surfactants- Polyvinylpyrrolidone (PVP), sodium dodecyl sulfate (SDS), and Gum Arabic (GA)- were assessed as stabilizers to prevent the graphene nanoplatelets from agglomeration and precipitation. It was found out that among them SDS was the most appropriate choice to keep the graphene nanoplatelets suspended for the reasonable time period which would allow the nanofluid emulsion to be injected to the molten polypropylene within the extrusion process.The recipe, fixed for all suspensions, was composed of four steps shown in Table 2.3.

Table 2.3. Ultrasonication and mechanical mixer process parameters for surfactant assessment.

Content	Process	Duration (min)
Water+surfactant	mechanical mixing 2000rpm	15
Water+ surfactant+ Graphene	mechanical mixing 2000rpm	90
Water+ surfactant+ Graphene	Sonication ~170 W	90
Water+ surfactant+ Graphene	mechanical mixing 1000rpm	15

Being chosen as an appropriate emulsion stabilizer, SDS was mechanically mixed with graphene nanoplatelets in the presence of water. Actually, a 0.2 gram SDS was added to the 100 ml water. After that, graphene nanoplatelets with the weight fraction of 3.5 wt.% were added to the water based solution followed by mechanical mixer for about 15-20 minutes. Finally, the obtained suspension was poured into the unlrasonication tank with 1.5 Litre liquid capacity and sonicated for about 90-120 minutes with 170 W power and 90-100% amplitude. During the sonication, the suspension was regularly circulated at 50-60 rpm and constantly kept cooled at 22 °C. The closed-circuit ultrasonication system was shown in Figure 2.12.

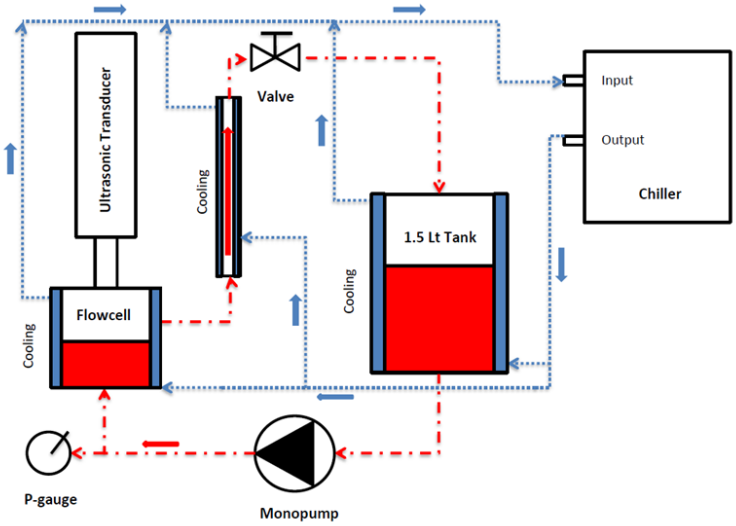

Figure 2.12. Closed-circuit ultrasonication system.

The sonicated nanofluids were then ready to be injected into the PP through the liquid feeder by the extrusion technique with the screw configuration dedicated to nanocomposite production. Screw configuration was the same as CB-PP nanocomposites [Figure 2.13]. Process parameters, however, were different from the previous experiments [Table 2.1., Table 2.2.]. In this experiment, xGnPs emulsion was transported into the the polypropylene by the liquid feeder at barrel location Z5. The position of main feeder, volumetric feeder, and the venting were the came as it had been arranged for composites shown in Figure 2.6. %4xGnPs-PP and %8xGnPs-PP nanocomposites were produced by adjusting the volumetric rate of the xGnPs emulsion.

As for the 4 percent graphene based PP nanocomposites, the nanofluid suspension with the 0.035 g/ml graphene nanoplatelets were fed into the PP through the liquid feeder. In order to have the exact weight percent of xGnPs, some calculations were needed. The extruder throughput was set to be $300g/h$ and in order to obtain 4 wt% nanocomposite, the gravimetric feeding rate of xGnPs should be $300g/h \times 0.04 = 12g/h$. To achieve this feeding rate for graphene nanoplatelets, the volumetric feeding rate of the suspension should be $12g/h \times 0.035\ g/ml\ = 343ml/hr$. The process was checked out for 5 minutes to 10 minutes intervals to see whether or not the correct combinations are mixed. After the viscosity of nanocomposite strings was reached, they were cooled in the water bath and then pelletized. The produced nanocomposite granules were then injected molded.

Similarly, preparation procedure for nanofluid suspension regarding the 8 percent graphene nanoplatelets PP nanocomposites was exactlty the same as 4 percent graphene patelets reinforced PP nanocomposites. The extruder throughput was set to be $200g/h$ and in order to obtain 8 wt% nanocomposite, the gravimetric feeding rate of xGnPs should be $200g/h \times 0.08 = 16g/h$. To achieve this feeding rate for graphene nanoplatelets, the volumetric feeding rate of the suspension should be $16g/h \times 0.035\ g/ml\ = 458ml/hr$.

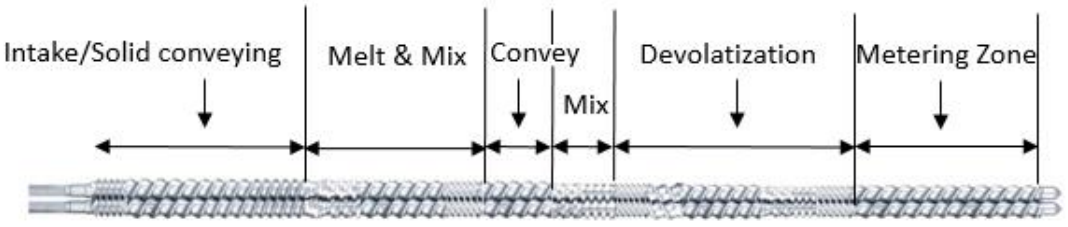

Figure 2.13. Screws configuration for xGnPs-PP nanocomposites.

2.3. Testing

Five different tests were carried out on composites and nanocomposites: Tensile testing, thermogravimetric analysis, melt flow index measurements, and conductivity measurements, and electrical property measurements.

2.3.1. Tensile Strength

The dog-bone shaped samples obtained from the injection molding process were aged at least for 48 hours and subjected to tension test. Tension test were carried out in Zwick/Roll Z010 tensile test machine with a load accuracy of 0.1%, and with the 10 kN load cell, shown in figure 2.14 according to the ISO-527 standard [88] and the tests parameters were summarized below at Table 2.4. Given the aforementioned standard, the dog-bone shaped samples were manufactured with the dimensions indicated in Table 2.5.

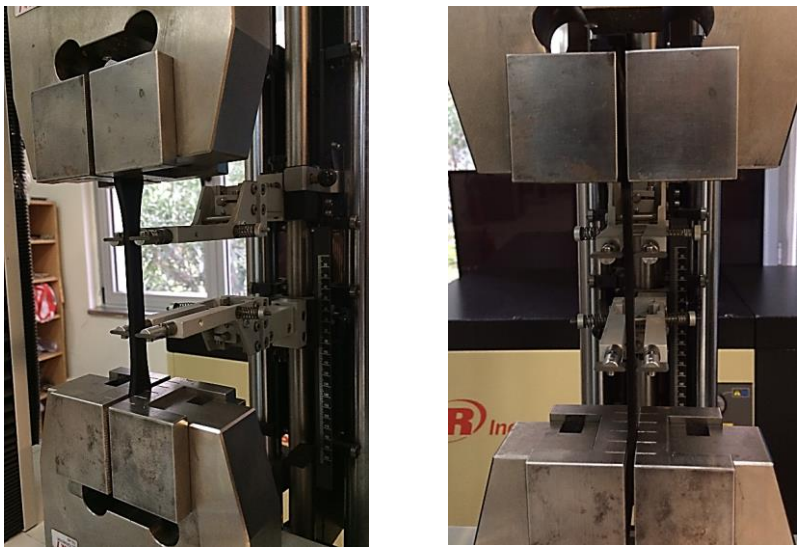

Figure 2.14. Tensile test set-up.

Table 2.4. Parameters of the tensile test according to the ISO527 [88].

Grip to grip separation at the start position	110 mm
Gauge length	75 mm
Pre-load	0.5 MPa
Speed- Preload	5 mm/min
Speed- Tensile Modulus	2 mm/min
Speed- After the yield strength point	50 mm/min
Force shutdown threshold	80% F_{max}
Begin of tensile modulus determination	0.05 ε%
End of tensile modulus determination	0.25 ε%

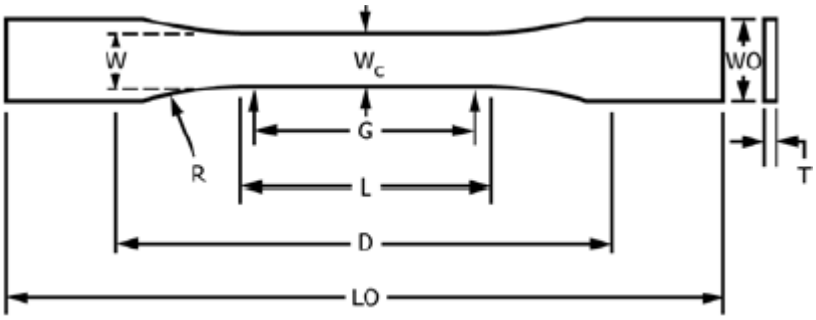

Figure 2.15. Schematic drawing of the tension test specimen [88].

Table 2.5. Specimen dimensions.

Width of narrow section (mm)	W	10
Length of narrow section (mm)	L	76
Width overall (mm)	WO	20
Length overall (mm)	LO	150
Gage length (mm)	G	75
Distance between grips (mm)	D	110
Radius of fillet (mm)	R	78
Thickness (mm)	T	4

2.3.2. Melt Flow Index Measurements

CB-PP and xGnPs-PP nanocomposites were analysed for their melt flow index at INSTRON CEAST MF20 melt flow index testing machine with an accuracy of 0.01 $^{g}/_{10\ min}$ according to the ASTM-D1238 standard [76], and the scematic view of the melt flow index test was illustrated in Figure 2.15. The test consists of the specification of the rate of extrusion of molten thermoplastic resins via an extrusion plastometer. Resin was extruded through the die with a specified orifice diameter and length under determined conditions such as piston position in the barrel, temperature, and load after a specified pre-heating time. Procedure B of ASTM-D1238 standard, which specifies automatically timed measurements were applied to each specimen. Melt flow rate (MFR- g/10min) and melt volume rate (MVR- cm^3/10 min) of thermoplastics were obtained.

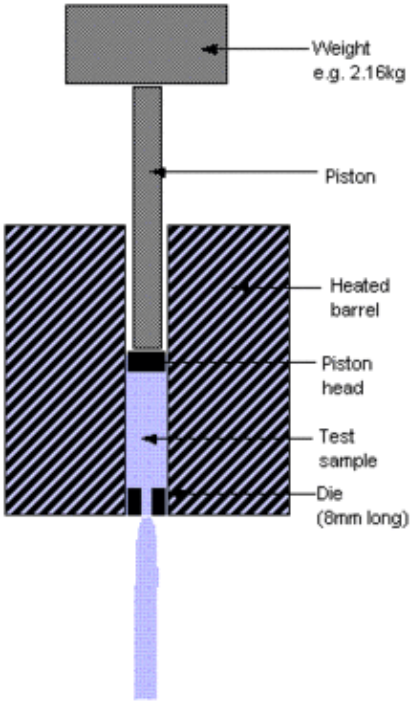

Figure 2.16. Melt Flow test set-up.

2.3.3. Scanning Electron Microscopy (SEM)

To understand distribution and dispersion of the nanofibers throughout the matrix qualitatively, the scanning electron microscopy (SEM) test was employed. Practically, SEM

uses a focused beam of high-energy electrons to produce different signals at the surface of solid specimens. In this regard, data is collected over a selected region of the sample's surface and then a two-dimensional image is created that displays spatial variations in properties including texture and orientation of materials. Before the test was begun, the samples obtained from the extrusion process with the Ø3x100 mm^3 volume had been prepared such that they first were cut manually and then undergone the crogenic process (freeze fractured) in order to create the fracture surface. After being broken, samples were sputter coated by platinum in order to enable or improve the imaging of samples in which the created conductive layer on the fracture surface inhibits charging, reduces thermal damage and improves the secondary electron signal required for topographic examination in the SEM. Finally, the Philips XL30 ESEM system shown in figure 2.16. was used to analyse the surfaces of samples.

Figure 2.17. Philips XL30 ESEM system.

2.3.4. Thermogravimetric Analysis (TGA)

Thermogravimetric analysis (TGA) is a thermal analysis techniques used to characterize the amount and rate (velocity) of change in the mass of a sample as a function of temperature or time in a controlled atmosphere. TGA were carried out for different amount of filler loadings including CB and graphene dispersed in the polypropylene matrix. TGA Q5000 V3.17 Build 265 was used for the analysis with an uncertainty level of 0.01 °C. The mass of the samples were approximately 9.4 mg and the test was begun from 24°C

(room temperature) up to 900 °C with 20°C increase in every minute under nitrogen athmosphere.

2.3.5. Electrical Property Measurements

In order to measure the electrical conductivity of the samples, Solartron analytical 1260 Impedance/Gain device, shown in Figure 2.17, was used such that the dog-bone shaped samples, which were produced via injection-moulding process, were cut into prsimatic shape with the dimension of $40 \times 10 \times 3.5$ mm^3. Then, they were all grinded to make sure that the upper and bottom surface of the samples are parallell with each other shown in Figure 2.18. The eight samples were silver coated and placed between two copper- cylindrical dies of the Solartron device [Fig.]. Each sample is tested for two times such that after the first loop finished, the second loop begun. The frequency ranges used in this process was between 10^{-1} and 10^{7} Hz. The potential was set to 100 V, and the electric current used in the experiments was the alternating current (AC).

Figure 2.18. Solartron analytical 1260 impedance/Gain device and placement of the silver-coated sample between two cylindrical copper parts.

Figure 2.19. Grinded samples ready to be silver coated.

3. RESULTS AND DISCUSSIONS

In this part of the thesis the mechanical and electrical, and rheological properties of the composites and nanocomposites are presented. The actual weight percent of the nanoparticles are measured by weight loss upon ignition measured in a TGA instrument.

3.1. Mechanical Properties

To better understand the mechanical behaviour of polymers, the typical stress-strain curves taken from the ISO-527 standard, is shown below in Figure 3.1. Given the graphs, the stress-strain parameters must be clearly explained. In this regard, stress at which the strain obtains the specific value x (%) is called stress at x % strain expressed as σ_x as a megapascal. Stress at which the sample breaks is called stress at break (σ_b) and its corresponding strain is the strain at break (ε_b). Strain at yield (ε_y) is the point at which the strain is started to increase without an increase in stress and its corresponding stress is expressed as σ_y. Nominal strain (ε_{tb} , ε_{tm}) is the last recorded data point at which the stress is decreased to less than or equal to 10% of the strength. Modulus (E_t) is the slope of the stress-strain curve between ε_1= 0.05% and ε_2= 0.25% strain intervals. Moreover, materials' stress-strain curve can be attributed to one the curves indicated in figure 3.1 in which curve a is for brittle materials, curve b and c is for tough materials with yield point, and finally curve d is for tough materials without yield point.

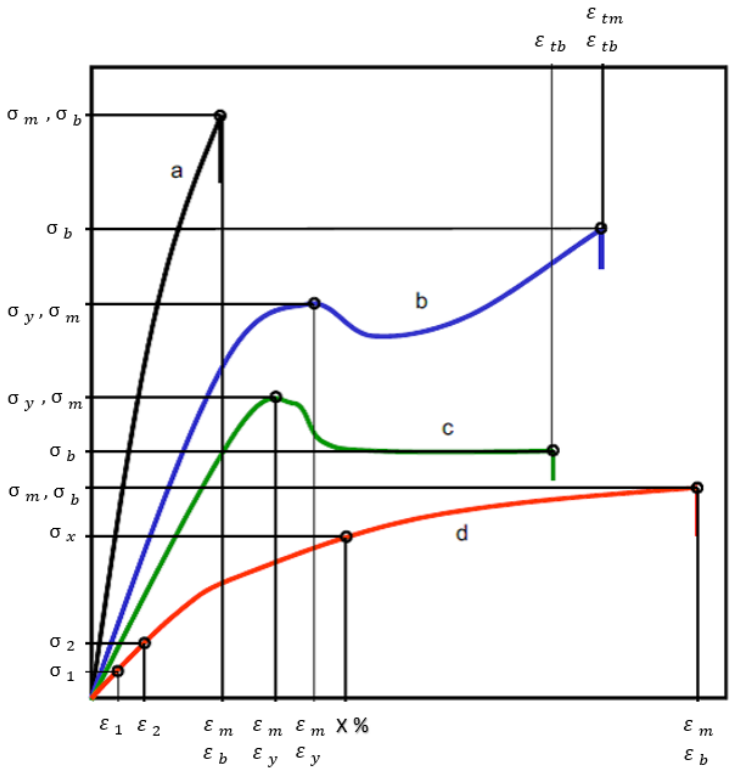

Figure 3.1. Typical stress-strain curves for polymers, reproduced from ISO 527-1 standard [88].

3.1.1. CF-PA6 composite

The results were presented in Tables 3.1 and 3.2, as well as Figures 3.2 and 3.3. The properties of the PA6/10CF composite were compared to those of the base polymer and the results demonstrated that addition of 10%CF results in a 10% increase in tensile strength, a 53.7% increase in tensile modulus, and a 71.0% decrease in strain at break when compared to neat PA6.

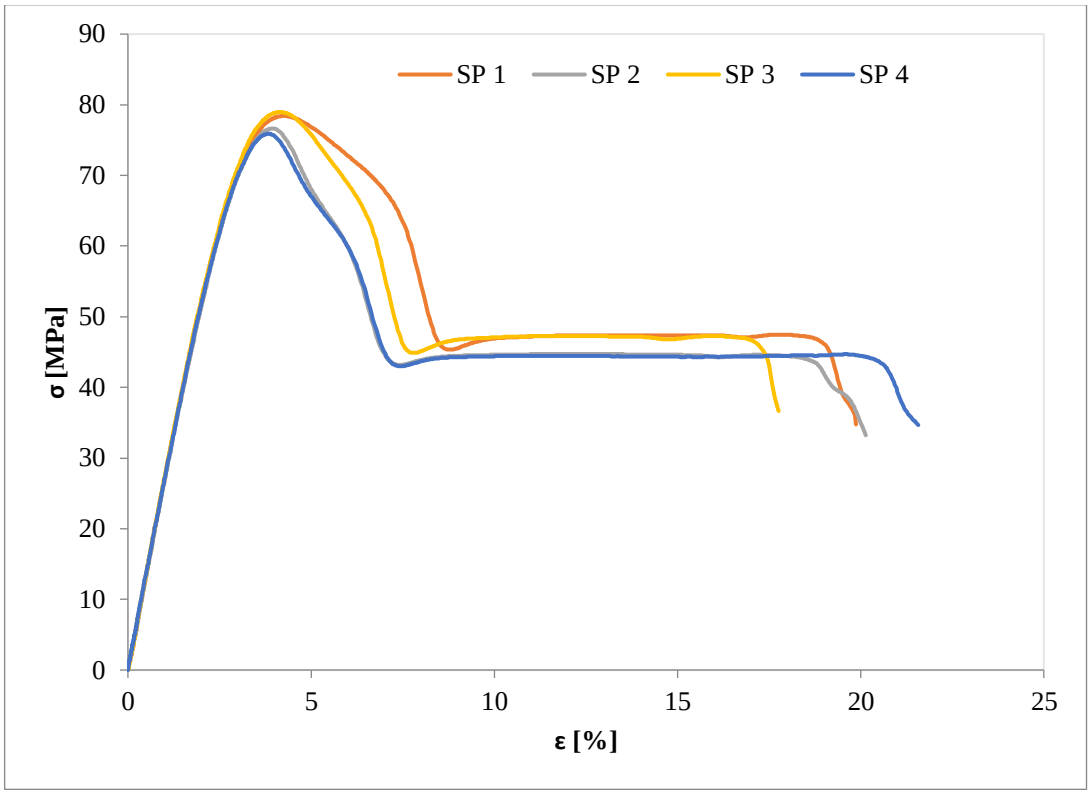

Figure 3.2. Stress-strain graphs of PA6 samples.

Table 3.1. Mechanical properties of neat PA6 Material.

Material	E_t	σ_Y	ε_Y	σ_M	ε_M	σ_B	ε_{tB}
-	MPa	MPa	%	MPa	%	MPa	%
SP-01	2603	78.4	4.2	78.4	4.2	34.7	19.7
SP-02	2558	76.6	3.9	76.6	3.9	33.2	19.7
SP-03	2691	78.9	4.1	78.9	4.1	36.6	17.8
SP-04	2628	75.8	3.8	75.8	3.8	34.6	20.9
Average	2620	77.4	4.0	77.4	4.0	34.7	20.5
Standard deviation	55	1.45	0.18	1.45	0.18	1.39	1.28

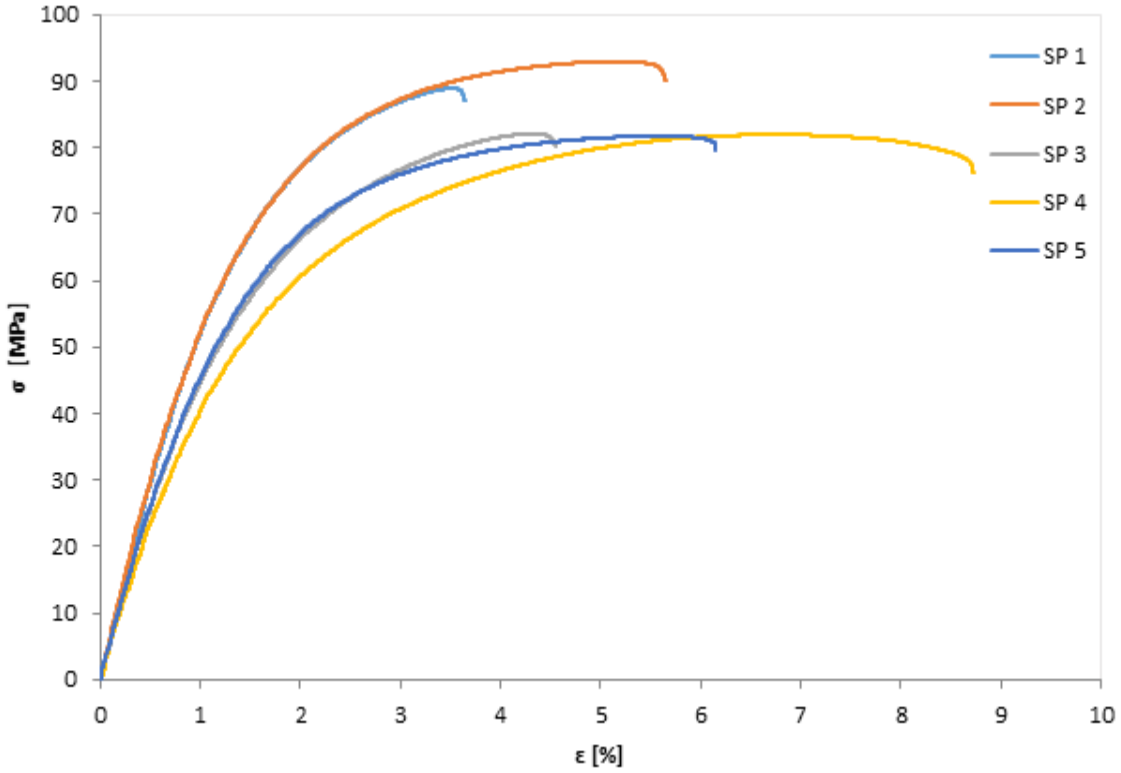

Figure 3.3. Stress-strain graphs of PA6/10CF samples.

Table 3.2. Mechanical properties of 10CF/PA6 composite.

Material	E_t	σ_Y	ε_Y	σ_M	ε_M	σ_B	ε_B
-	MPa	MPa	%	MPa	%	MPa	%
SP-01	6304	-	-	88.8	3.5	88.8	3.5
SP-02	6270	-	-	92.9	5.2	92.9	5.2
SP-03	5513	-	-	82.1	4.3	82.1	4.3
SP-04	4886	81.9	6.6	81.9	6.6	76.2	8.7
SP-05	5335	81.7	5.4	81.7	5.5	79.6	6.1
Average	5662	81.8	6.0	85.5	5.0	83.9	5.6
Standard deviation	615	0.141	0.84	5.12	1.2	6.83	2.0

3.1.2. CF-PP Composites

In the second place, both neat PP and 20CF/MA-g-PP/PP composites were subjected to tensile test and it was found out that the mechanical properties of the base polymer which in this case was polypropylene was not so much affected by adding the carbon fibres. In order to have the good interfacial interaction between carbon fibres and polypropylene,

maleic anhydride grafted polypropylene was used to guarantee the better transformation of the properties from the fibres to the polymer. Modulus of elasticity of the composite increased about 340% whereas the strain at break extremely decreased about 98%. Also, the ultimate stress of the composites exhibited no change acoording to the results shown in Figure 3.4, 3.5, and Tables 3.3, 3.4.

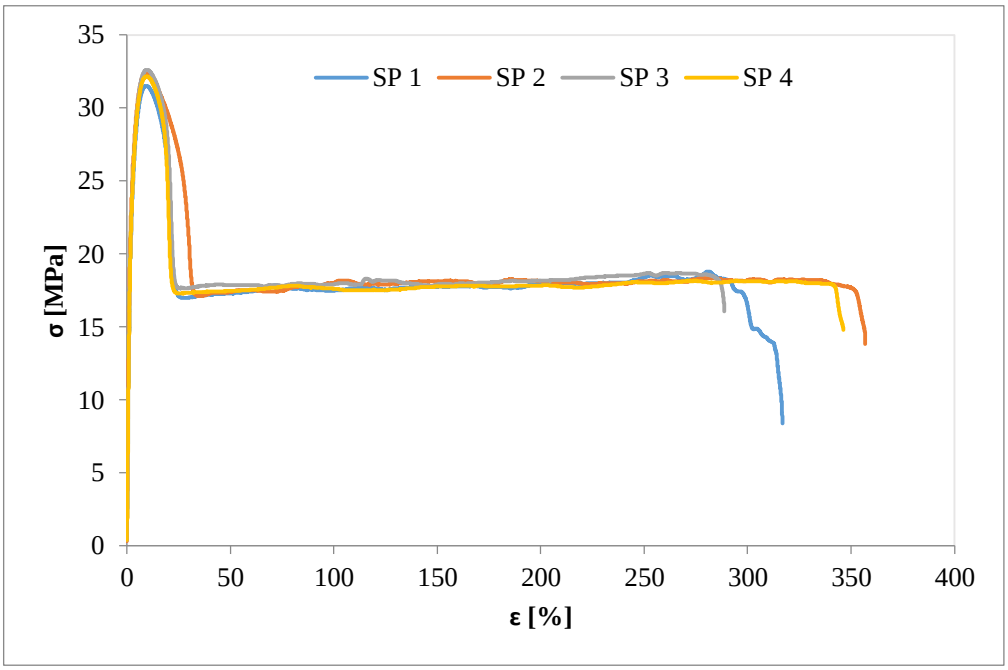

Figure 3.4. Stress-strain graphs of PP samples.

Table 3.3. Mechanical properties of neat PP.

Material	E_t	σ_Y	ε_Y	σ_M	ε_M	σ_B	ε_{tB}
-	MPa	MPa	%	MPa	%	MPa	%
SP 1	1334	31.5	9.1	31.5	9.1	8.38	310.6
SP 2	1546	32.4	9.4	32.4	9.4	13.8	350.8
SP 3	1371	32.6	9.7	32.6	9.7	16.0	272.7
SP 4	1415	32.2	9.3	32.2	9.3	14.8	330.2
Average	1416	32.1	9.4	32.1	9.4	13.2	316.0
Standard deviation	94	0.471	0.25	0.471	0.25	3.42	33.27

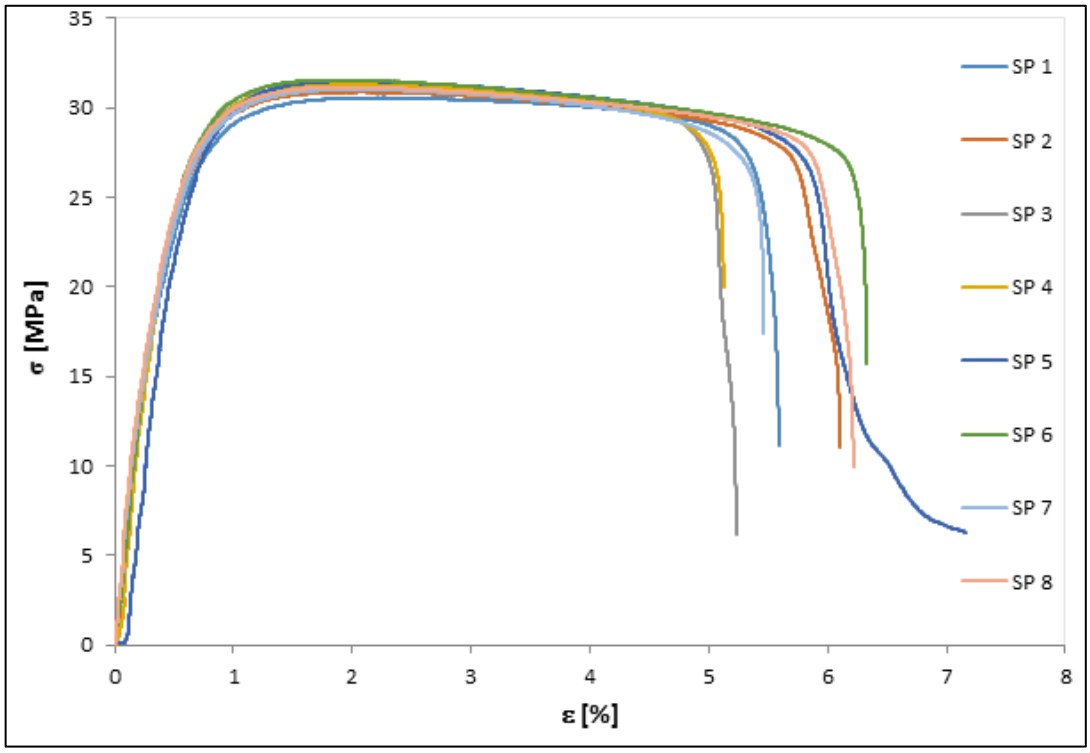

Figure 3.5. Stress-strain graphs of 20CF/MA-g-PP/PP sample.

Table 3.4. Mechanical properties of 20CF/MA-g-PP/PP composite.

Material	E_t	σ_Y	ε_Y	σ_M	ε_M	σ_B	ε_B
-	MPa	MPa	%	MPa	%	MPa	%
SP 1	6060	30.6	2.2	30.6	2.2	11.1	5.6
SP 2	6671	30.8	2.1	30.8	2.1	11.1	6.1
SP 3	5848	31.3	1.8	31.3	1.8	6.14	5.2
SP 4	7060	31.3	1.8	31.3	1.8	19.9	5.1
SP 5	5735	31.5	1.9	31.5	1.9	6.29	7.1
SP 6	6381	31.5	1.8	31.5	1.8	15.7	6.3
SP 7	5952	31.0	2.1	31.0	2.1	17.4	5.5
SP 8	6206	31.1	1.8	31.1	1.8	9.95	6.2
Average	6240	31.1	1.9	31.1	1.9	12.2	5.9
Standard deviation	448	0.323	0.17	0.323	0.17	5.00	0.65

In CF-PP composites, the modulus of elasticity increased about 340%, and the tensile strength value did not sinficantly change while the strain at break decreased enormously as compared to the neat PP . CF-PA6 composite, on the other hand, demonstrated slight (about 10%) increase in the tensile strength and 53,7% increase in the modulus of elasticity whereas the strain at break decreased about 71%. Therefore, polymers' flexibility and elongation

under the tensile loading are hugely affected by adding the carbon fibres as demonstrated in Figure 3.6.

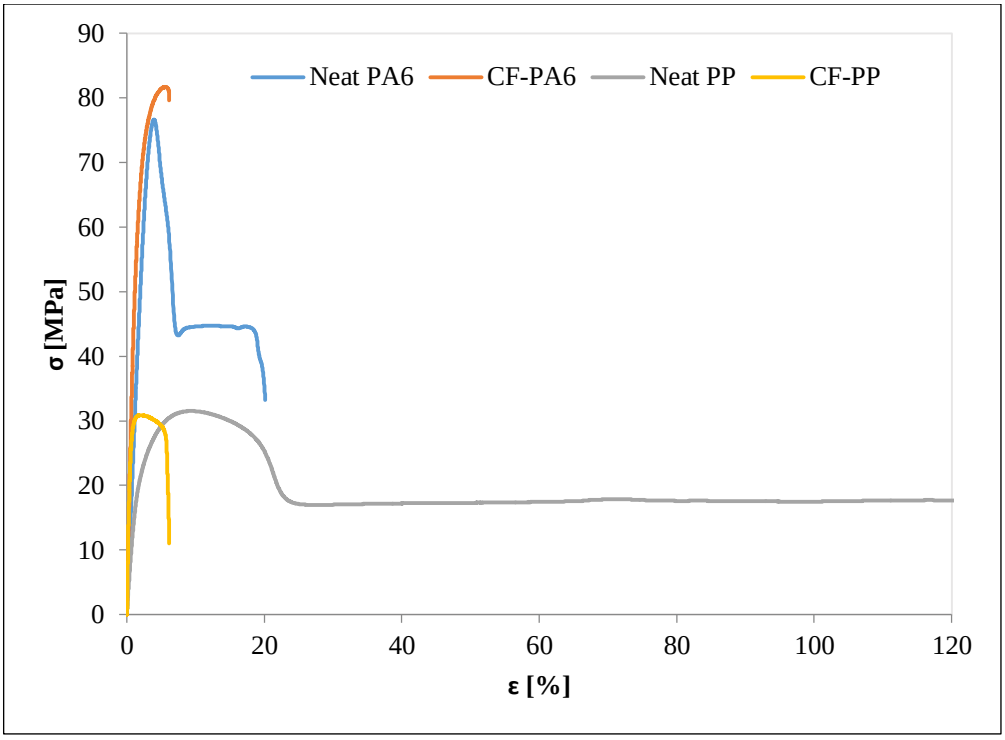

Figure 3.6. Stress-strain graphs of CF-PP and CF-PA6 as well as neat PP and PA6.

3.1.3. CB-PP Nanocomposites

The CB-PP nanocomposites with four different weight fractions were subjected tensile tests. PP used in nanocomposites was the same as the one used for CF-PP composite. As illustrated in Figure 3.7, by increasing the nanoparticles loading, mechanical properties of the polypropylene have been significantly compromised such that 40 per cent CB has decreased the ultimate strength of the base polymer up to 46.8% and strain at break up to 99.7% whereas the modulus of elasticity increased about 37.8%.

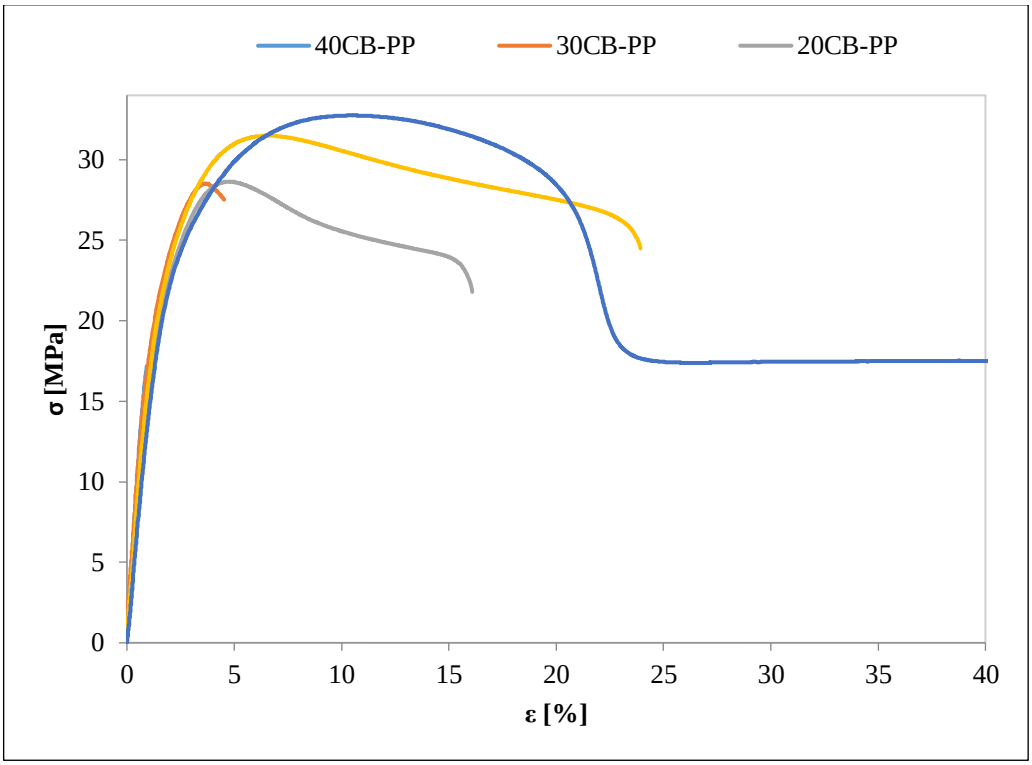

Figure 3.7. Stress-strain curves of CB-PP nanocomposites and neat PP.

3.1.4. xGnPs-PP Nanocomposites

Finally, as illustrated in figures 3.8, 3.9 and tables 3.5, 3.6, xGnPs-PP nanocomposite were subjected to tensile tests and it was found out that none of the graphene based PP nanocomposite have improved mechanical properties in comparison to the neat polymer. Also, both nanocomposite samples- 4 wt.% and 8 wt.%- have significantly different mechanical properties.

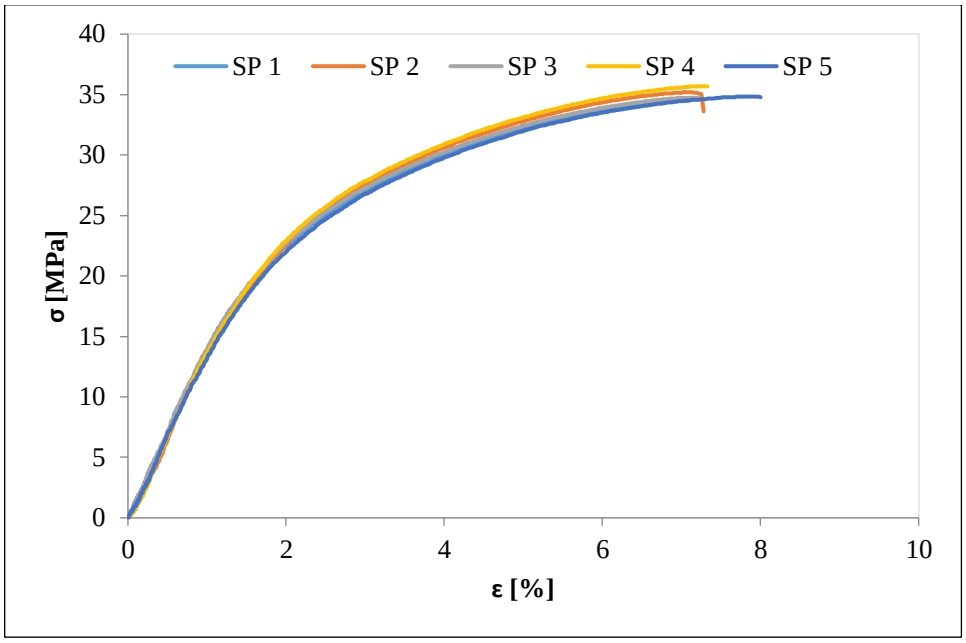

Figure 3.8. Stress-strain graphs of 4xGnPs-PP samples.

Table 3.5. Mcehnaical properties of 4xGnPs-PP nnaocomposites.

Material	E_t	σ_M	ε_M	σ_B	ε_B
-	MPa	MPa	%	MPa	%
SP 1	1289	34.5	7.0	34.5	7.0
SP 2	1251	35.1	7.0	35.1	7.0
SP 3	1386	34.7	7.1	34.7	7.1
SP 4	1191	35.7	7.3	35.7	7.3
SP 5	1252	34.8	7.8	34.8	7.8
Average	1274	34.9	7.2	34.9	7.2
Standard deviation	72	0.461	0.33	0.461	0.33

Overall, the exfoliated graphene nanoplatelets based PP (xGnPs-PP) nanocomposites are compared with CB based PP (CB-PP) nanocomposites. The resulting nanocomposites are also compared to neat polypropylene. As illustrated in figure 3.10, with small amount of graphene loading about 4 wt.% or 8 wt.%, xGnPs-PP nanocomposites demonstrate even better mechanical properties than 10CB-PP nanocomposites. Increasing the amount of CB particles in the PP compromise the mechanical properties of the base polymer. For example, the tensile strength and strain at break for all CB loading are reduced. It can be one of the three factors may cause a reduction in strength: agglomeration, low degree of dispersion, or poor polymer-matrix cohesion. Dispersion seems to be uniform when fracture surfaces of the nanocomposites are examined, however, one cannot come to a conclusion about

filler/matrix interface since the magnification is not sufficient. In both nanocomposites, the strain at break are decreased significantly in comparison to the neat polymer which reaches its minimum value at 40% CB loading.

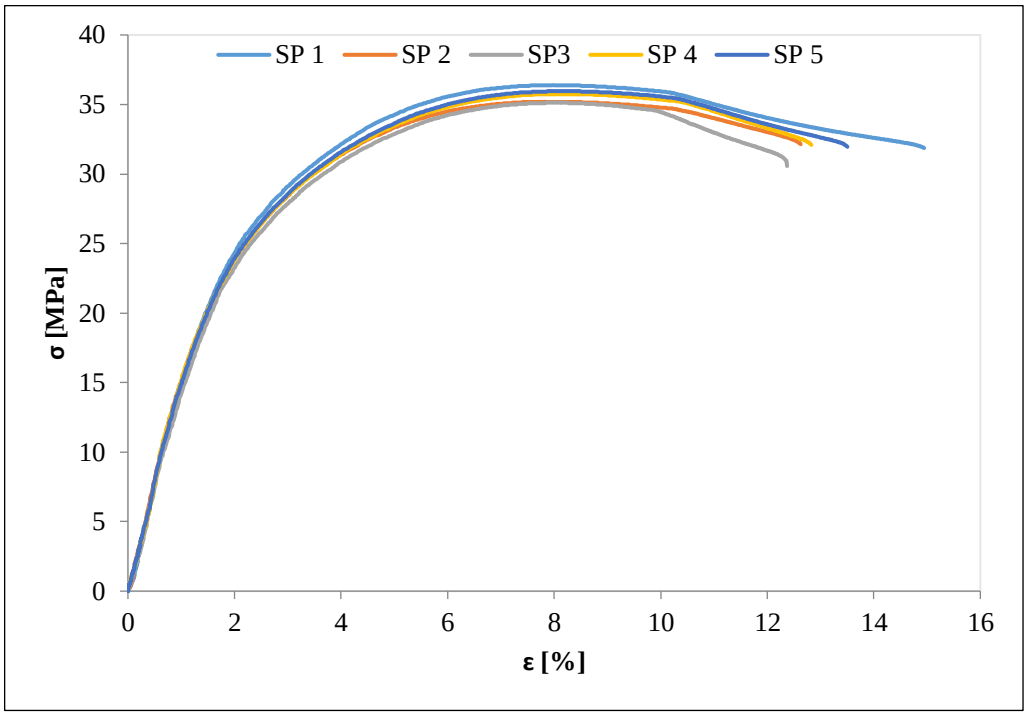

Figure 3.9. Stress-strain graphs of 8xGnPs-PP samples.

Table 3.6. Mechanical properties of 8xGnPs-PP % nanocomposites.

Material	E_t	σ_Y	ε_Y	σ_M	ε_M	σ_B
-	MPa	MPa	%	MPa	%	MPa
SP 1	1562	36.4	7.9	36.4	7.9	31.8
SP 2	1730	35.2	7.8	35.2	7.8	32.1
SP 3	1212	35.1	8.1	35.1	8.1	30.6
SP 4	1371	35.7	8.1	35.7	8.1	32.1
SP 5	1445	35.9	8.1	35.9	8.1	31.9
Avergae	1464	35.6	8.0	35.6	8.0	31.7
Standard deviation	195	0.532	0.14	0.532	0.14	0.621

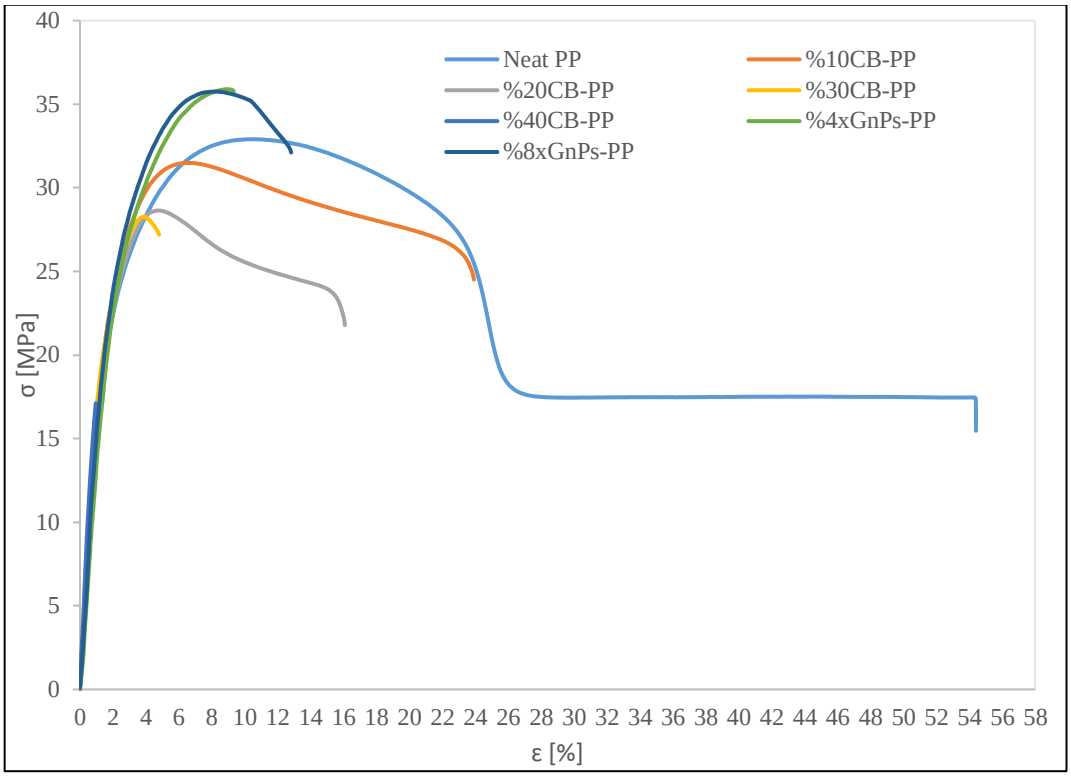

Figure 3.10. Stress-strain curves of CB-PP and xGnPs-PP nanocomposites.

3.2. Rheological Properties

3.2.1. Melt Flow Index

The CB-PP and xGnPs-PP nanocomposites were all assessed for their melt flow rate at the same temperature condition, which was 230℃. Considering the melt flow index shown in Table 3.7, by increasing the amount of nanoscale materials in the polymeric matrix, the melt flow index was decreased proving that the viscosity of the nanocomposite had been raised as expected.

Table 3.7. Melt Flow indexes of nanocomposites according to the ASTM-D1238 [89].

Material	Specification	MFR-A (gr/10 min)	MFR-B (gr/10 min)	MVR (cm^3/10 min)	Time Interval (min)
PP	PP-01	23.39	26.89	31.56	0.5
	PP-02	28.59	32.89	38.60	
	PP-03	30.19	35.88	42.12	
	PP-04	23.19	26.72	31.36	
	PP-05	27.59	31.91	37.45	
	Average	26.59	30.86	36.22	
	Standard deviation	3.12	3.91	4.71	
10% CB + PP	CB-01	18.12	21.61	23.76	0.5
	CB-02	19.82	23.42	23.76	
	CB-03	20.66	24.55	27.01	
	Average	19.53	23.19	24.84	
	Standard deviation	1.33	1.52	1.82	
20% CB + PP	CB-01	9.82	11.40	12.31	0.5
	CB-02	9.35	11.40	12.31	
	CB-03	9.51	11.40	12.31	
	Average	9.56	11.40	12.31	
	Standard deviation	0.21	0.00	0.00	

Table 3.7. Melt Flow indexes of nanocomposites according to the ASTM-D1238 [89].

Cont.

Material	Specification	MFR-A (gr/10 min)	MFR-B (gr/10 min)	MVR (cm^3/10 min)	Time Interval (min)
30% CB + PP	CB-01	2.45	3.01	3.08	3.0
	CB-02	3.47	3.86	3.97	
	CB-03	2.73	3.05	3.14	
	Average	2.88	3.30	3.39	
	Standard deviation	0.52	0.48	0.49	
4% xGnPs + PP	xGnPs-01	21.78	24.46	28.32	0.5
	xGnPs-02	23.16	26.82	31.57	
	xGnPs-03	23.24	26.91	31.78	
	Average	22.73	26.06	30.56	
	Standard deviation	0.82	1.41	1.93	
8% xGnPs + PP	xGnPs-01	19.56	23.24	24.96	0.5
	xGnPs-02	20.65	24.57	27.18	
	xGnPs-03	18.36	22.14	24.13	
	Average	19.52	23.32	25.42	
	Standard deviation	1.12	1.24	1.62	

3.3. Scanning Electron Microscopy (SEM)

As obtained by the SEM test and shown in Figure 3.11, the graphene nanoplatelets were accumulated on top of each other, and the accumulation was increased by an increase in the filler loading. Also, it was observed that the xGnPn-PP nanocomposites had gotten rich and poor graphene distributed regions. The degree of the dispersion for xGnPs-PP nanocomposites is not as good as the CB-PP ones since the fibre nanoplatelets' pull-out has been seen. In some region of the xGnPs-PP nanocomposites, the wrinkled/tubed/folded nanoplateletes has been observed as well. All of the aforementioned observations could have significantly influence mechanical properties nanocomposites.

Despite all the unexpected behaviours seen in the xGnPs-PP nanocomposites, the CB-PP nanocomposites demonstrate the homogenous distribution throughout the polymer.

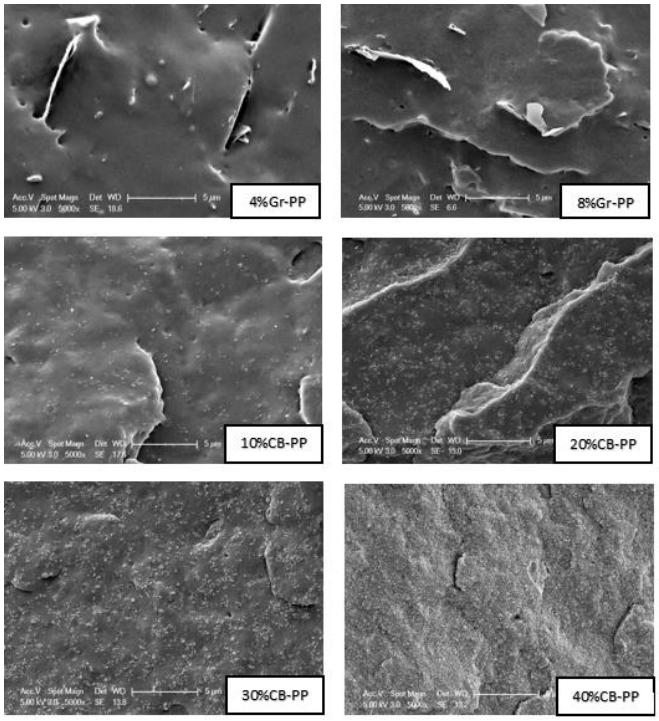

Figure 3.11. Scanning electron microscopy of nanocomposites with various nanofiber fractions magnified at 5000x.

3.4. Termogravimetric Analysis (TGA)

The thermogravimetric analysis was performed for CB-PP and xGnPs-PP nanocomposites under nitrogen athmosphere in order to find the mass residue. The results were summarized at Table 3.8 and Figure 3.12. The mass residue fraction at 700 ^{o}C is slightly less than expected. Only a single measurement was performed and the sample could be taken from a filler poor region, and if multiple samples are used, the residue fraction, which is basically carbon nanoparticles can come up to the nominal value. Given the initial degradation temperature, xGnPs-PP nanocomposites demonstrated an improvement in its thermal stability by adding nanoplatelets loading whereas CB-PP nanocomposites' thermal stability were decreased by increasing the amount of nanoparticulates. This observation could be related to the thermal capacity of the CB-PP nanocomposites. In other words, the less the thermal capacity of the nanocomposites, the less they could store heat per unit

volume which would also increase the heat flow of a sample or vice versa. Therefore, it could be understood that the heat flow of the CB-PP nanocomposites were increased by increasing the nanofiller loading resulting in the decrease in both the thermal stability and thermal capacity.

Table 3.8. Thermal degradation parameters obtained by TGA of nanocomposites.

Sample	$T_{2\%}$ (°C)	Major weight loss peak temperature (°C)	Mass residue (%)
10%CB-PP	399.15	447.90	8.90
20%CB-PP	328.05	447.57	17.1
30%CB-PP	306.16	446.44	25.1
40%CB-PP	269.30	445.53	34.0
4%xGnPs-PP	345.81	432.51	3.12
8%xGnPs-PP	399.25	443.62	8.91

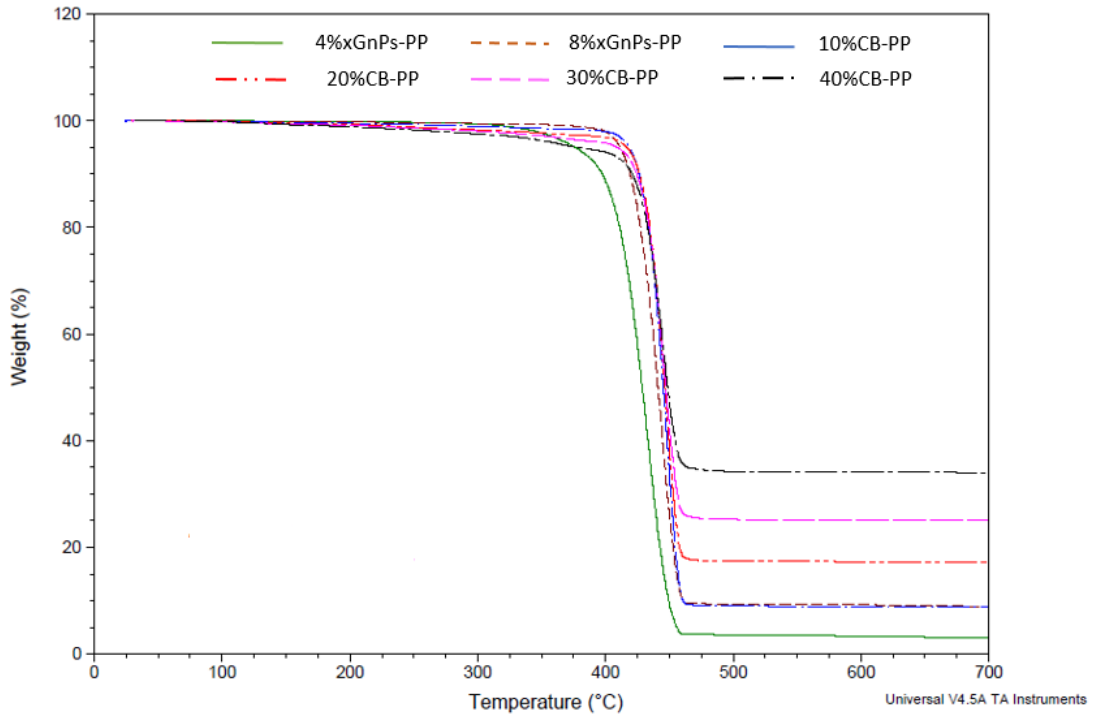

Figure 3.12. TGA curves of nanocomposites.

3.5. Electrical Property Measurements

In general, the setups used to measure the conductivity of materials demonstrates the conductance in terms of surface/volume resistivity. Volume resistivity is inverse of the electrical conductivity and defined as the resistance through a unit cube of a material. As expressed in ohm.cm, it would be the electrical resistance through a one-centimeter cube of a material. Volume resistivity is deemed as an important factor when it deals with the bulk materials, such as charge storage and EMI shielding. Therefore, the volume resistivity can be calculated from the following formula in which ρ_v is the volume resistivity, R is the resistance measured in ohms ($\frac{Voltage}{Current}$), A is the area of a sample, and t is the average thickness of the sample:

$$\rho_v = \frac{RA}{t} \tag{3.1}$$

Resistance (real impedance) of both the graphene based polypropylene nanocomposite and the carbon black based polypropylene nanocomposites were measured after silver coating the samples for measuring their volume conductivity. During the experiments, the samples were subjected to alternationg currents of different frequencies with different current density but constant potential so that their conductivities under different conditions could be studied. Since the test results were in the form of impedance versus frequency, the resistivity of the samples were first calculated by the above formula. To obtain the conductivity for each sample in different frequencies, the resistivity value for each sample was inversed. In this regard, the first experiment was corresponded to the graphene based polypropylene nancomposites which proved that the materials behaviour are extremely affected by increasing the frequency such that materials resistance are being decreased in comparison with starting frequency point, on the whole. However, given the real impedance versus frequency curve shown in figure 3.13, two unexpected results were obtained: the first one was the discontinuity of points in some frequency domains which its highest magnitude was observed between 1.0 Hz and 100 Hz; the second one was the drastic real impedance peaks in some frequencies. The discontinuity issue can be related to the low frequency rate which means that the number of passing currents in a certain period of time is low and the corresponding current length is long which cannot catch the pulse of nanofillers and they

must have been imbedded in much more shorter distance to each other so that the length of the passing current could not encompass them. However, considering the second one, the observations seem peculiar and cannot be explained clearly.

The second phase of the experiment was related to the carbon black based polypropylene nanocomposites which almost demonstrated the rational behaviour in comparison with the graphene based polypropylene nanocomposites. As shown in figure 3.14, given the %10CB-PP nanocomposite, the reasons which have already been discussed for xGnPs-PP nanocomposites can be considered for it as well. Moreover, according to the obtained 3.14 impedance-frequency curves, the samples resistance demonstrated small dependency on frequency at high nanoparticles loadings such as 20%, 30%, and 40% CB-PP nanocomposites. To better understand the conductive characteristic of the CB-PP nanocomposites, the inverse of the resistivity value obtained in formula 3-1, which gives conductivity value, was calculated for certain frequency values to see wheter or not samples are either conductive or semiconductive, or insulator. By increasing weight fraction of nanoparticles in polymeric matrix, three of them-10% CB-PP, 20%CB-PP, and 30%CB-PP-were placed in the domain of semiconductive materials while the last one which had a 40% carbon black loading was proven to be the conductive sample.

Comparing two groups together, it is seen that even the lowest carbon black embedded in the polypropylene matrix has the lower resistance than a 4% graphene based polypropylene nancomposites. We believe that the lower electrical property of the graphene based polypropylene nanocomposites could be due to either agglomarate formation of nanoplatlets or the destruction of the graphene layer's honeycomb structure. In fact, to constitute the electrical network throughout the matrix, graphene nanoplatelets must have been in an insufficient distance which prevented them from exchanging the electrons via tunneling or jumping as the current passed through the samples' volume. Also, the accumulation of nanofibres throughout the matrix could have inhibited a good formation of electrical network since it has already been proved that the less accumulated the graphene layers on top of each other, the better their electrical properties could be. Besides, the ultrasonication process of the nanofluids could have affected the nanofibres properties such that if the timing and the power of the device was excessive, graphenes' hexagonal structure could be destroyed.

All in all, the electrical resistance results for both xGnPs-PP and CB-PP nanocomposites were listed at Table 3.9, and plotted against nanofiller concentration in Figures 3.13 and 3.14. Considering the CB-PP nanocomposite, the electrical percolation threshold was obtained at 20% CB nanoparticle loading. On the contrary, although xGnPs-PP nanocomposites demonstrated more or less electrical conductivity in some frequency domains, the electrical percolation threshold could not clearly been identified between two different nanaplatelet loading concentrations.

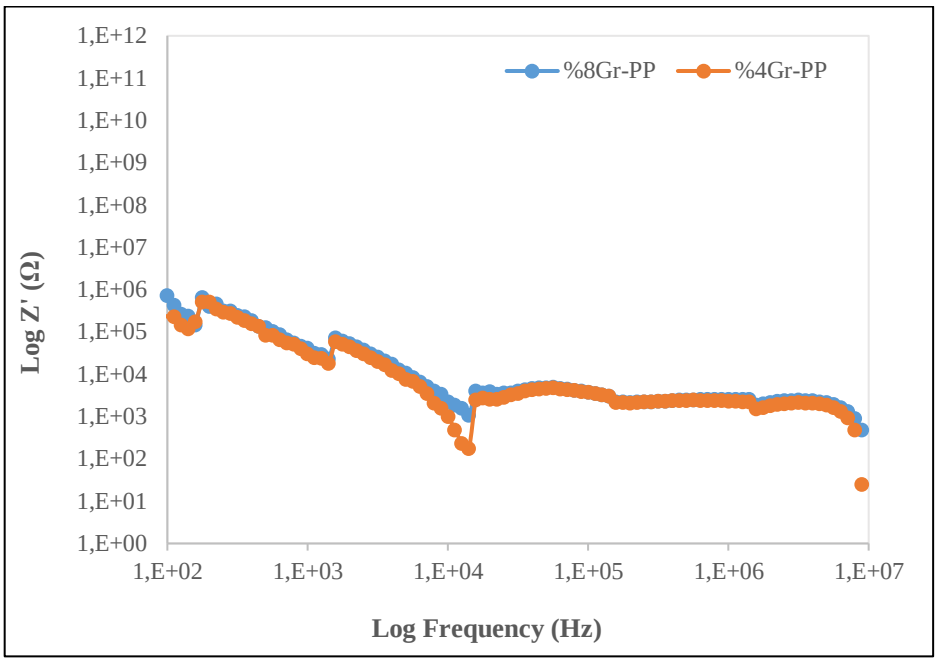

Figure 3.13. Real impedance (Z') vs. frequency of xGnPs/PP nanocomposites as a function of graphene weight fraction.

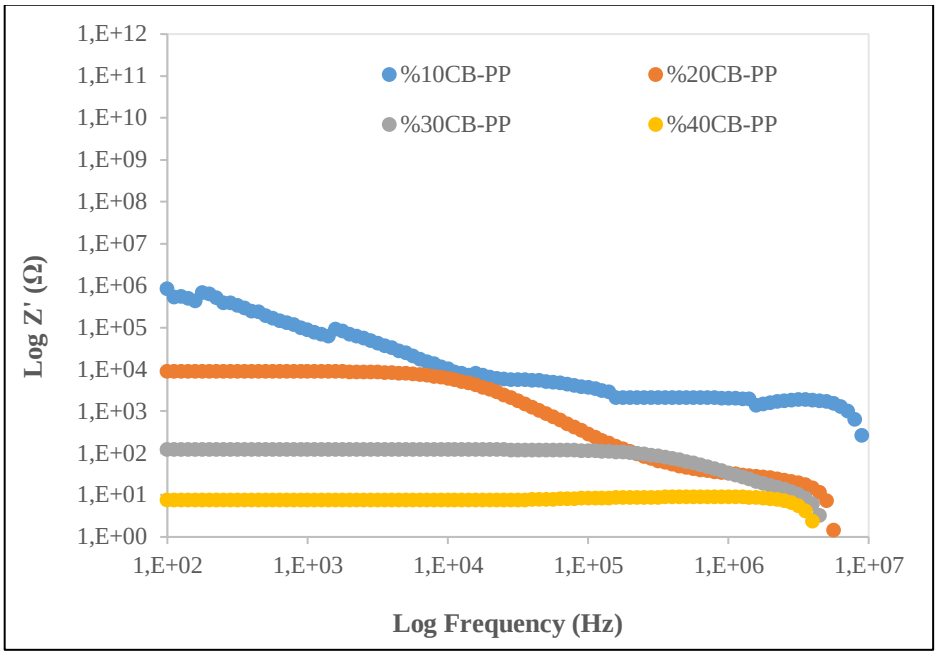

Figure 3.14. Real impedance (Z') vs. frequency of CB/PP nanocomposites as a function of CB weight fraction.

Table 3.9. Conductivity of the nanocomposites with different fibre loading in various frequencies.

	σ_1 (S/cm)	σ_{10} (S/cm)	σ_{10}^2 (S/cm)	σ_{10}^3 (S/cm)	σ_{10}^4 (S/cm)	σ_{10}^5 (S/cm)	σ_{10}^6 (S/cm)
4% xGnPs-PP	-	-	-	$\sim 10^{-4}$	$\sim 10^{-3}$	$\sim 10^{-3}$	$\sim 10^{-3}$
8% xGnPs-PP	-	-	-	$\sim 10^{-4}$	$\sim 10^{-3}$	$\sim 10^{-3}$	$\sim 10^{-3}$
10% CB-PP	-	-	-	$\sim 10^{-4}$	$\sim 10^{-3}$	$\sim 10^{-3}$	$\sim 10^{-3}$
20% CB-PP	$\sim 10^{-3}$	$\sim 10^{-3}$	$\sim 10^{-3}$	$\sim 10^{-3}$	$\sim 10^{-3}$	$\sim 10^{-2}$	$\sim 10^{-1}$
30% CB-PP	$\sim 10^{-2}$	$\sim 10^{-2}$	$\sim 10^{-2}$	$\sim 10^{-2}$	$\sim 10^{-2}$	$\sim 10^{-1}$	$\sim 10^{-1}$
40% CB-PP	$\sim 10^{+1}$	$\sim 10^{+1}$	$\sim 10^{+1}$	$\sim 10^{+1}$	$\sim 10^{+1}$	$\sim 10^{+1}$	$\sim 10^{+1}$

4. CONCLUSION AND FUTURE WORK

Exfoliated Graphene Nanoplatelets (xGnPs) and Carbon Black (CB) filled polypropylene samples were produced by melt mixing technique. xGnPs were exfoliated in the water-SDS solution by ultrasonication process while the CB-PP masterbatch were purchased and then melt mixed by polypropylene without any surface processing in various proportions. Both nanocomposite groups were analysed and examined to better understand the mechanical, rheological, thermal, and electrical characteristics of the products.

Considering the mechanical properties of the nanocomposites, the ultimate strength and stiffness of the xGnPs-PP samples were increased whereas the toughness and the strain at break were decreased in comparison with the neat polypropylene. However, compared with CB-PP nanocomposite samples, xGnPs-PP nanocomposite samples illustrated better mechanical properties even at the lowest graphene loading 4%.

CB-PP nanocomposites, on the other hand, demonstrated a decrease in mechanical properties as compared to the base polymer even at 10% nanofiller weight fraction. By increasing the nanofiller loading, the mechanical properties of the nanocomposites such that toughness, ultimate strength, strain at break were compromised compared to the neat polymer, although the stiffness was increased.

Given the rheological properties, as compared to neat polypropylene, CB-PP nanocomposite samples showed a decrease in the melt flow rate by increasing the nanofiber loading, which proved that a 40%CB-PP samples are more viscous than the neat polymer and CB-PP nanocomposites. Moreover, xGnPs-PP nancomposite samples exhibited the same same trend in rheological behaviour as CB-PP nanocomposites in which a decrease in the melt flow rate was observed by increasing the xGnPs fraction in the polymeric matrix.

As with the thermal properties of the nanocomposites, the xGnPs-PP samples demonstrated higher decomposition temperature shift by an increase in the amount of graphene nanoplatelets weight fraction in the polypropylene matrix The aforementioned

thermal stability improvement can be attributed to the homogenously distributed graphene that acts as a so-called “tortuous path” to decrease the diffusion of volatile decomposition products and slow down the release of these products. As with the CB-PP nanocomposites, their initial and maximum decomposition temperature were decreased by increasing the nanofiber weight fractions, which could be due to the excellent thermal stability and thermal conductivity of carbon black (CB), which perform as a heat sink to create thermal decomposition at a higher loading. Besides, a higher carbon black loading damages the micro-phase separation structure, which led to a reduced thermal stability. Therefore, from 10% CB loading to 40% CB loading, the initial and maximum decomposition temperatures were decreased up to 48,2 and 0,5%, respectively. As for the scanning electron microscopy, graphene platelets seem to have been distributed all over the matrix althouth there are regions with both poor and rich amount of graphene platelets. Moreover, indications of pulled-out nanoparticles are observed pointing out weak interfacial interaction and degree of dispersion between nanofillers and polymeric matrix. Besides, the wrinkled and folded nanoplatelets are also seen in some regions of the matrix. On the contrary, it is observed that carbon black nanoparticles are dispersed and distributed homogenously throught the matrix.

Considering the electrical resistance of the nanocomposites, exfoliated graphene nanoplatelets (xGnPs) based polypropylene (PP) illustrates both discontinuity in low frequency domains which has corresponded to the long current waves length passing through the sample and drastic resistance peaks due to the skin effect theory caused by the alternating current in the certain thickness of sample surface resulting in an increased current density in the regions close to the surface of the sample. However, by increasing the frequency, the samples electrical resistance started to decline. So, the frequency dependence of the xGnPs-PP nanocomposites at room temperature cannot be ignored. Furthermore, since the the distribution and dispersion of the nanoplatelets in the polypropylene has not been quite well, considering the fact that there has been agglomerates and wrinkled/folded platelets in the matrix according to the SEM tests, the electrical resistance results are not quite different between two nanofiller loadings- 4% xGnPs-PP and 8% xGnPs-PP. Therefore, uneven distribution of the nanofibres in the matrix has significantly affected the electrical resistance of the nanocomposites; also, increasing the frequency might have caused the polymers motion to be accelerated facilitating the disruption of the electrical network in an inhomogenous nanocomposites.

Comparing the summary of Li et al. research with our findings, it is seen that in the aforementioned work, most of the nanofibers are surface-processed before being integrated by the polymeric matrices which affected the properties of final product significantly. Among those findings summarized in the literature review section, the ones that had been produced by the in-situ polymerization or solution intercalation techniques demonstrated lower percolation threshold than the ones produced by melt mixing methods. Moreover, nanocomposites, having been produced by melt mixing method, had gone through different processing techniques prior to melt mixing such as surface modification or functionalization resulting in the lower electrical percolation threshold. Carbon black based polypropylene nanocomposite, on the other hand, shows a relatively homogenous distribution and dispersion which led to a percolation threshold which is at 20% loading. A 40% CB-PP is also categorized among the conductive materials for all range of frequencies.

As far as the objective of this study concerned, addition of conductive nanoscale materials such as graphene nanoplatlets have resulted in the conductive polypropylene nanocomposites by melt blending technique. It has also found that the existence of the exfoliated graphene nanoplatlets has not decreased the mechanical properties of nanocomposites up to 8% nanofiller loading with respect to the neat polypropylene. Electrical conductivity of the nanocomposites have been achieved at a frequency greater than 10^3 hz for both 4% and 8% exfoliated graphene nanoplates. CB-PP masterbatch nanocomposites, on the other hand, demonstrated electrical conductivity even at low frequencies with 20% which is also a percolation threshold, 30%, and 40% carbon black loading.

To sum up, functionalization or surface modification of the graphene nanoplatelets could have had significant effect on mechanical, rheological and electrical properties of the polymeric nanocomposites. For future work, ultrasonication process must be closely examined since it could have damaged the graphene plateletes' lamellar structures compromising their ability in transferring properties into the polymeric matrices during different mixing methods. Besides, the effect of sodium dodecyl sulfate as a compatibilizer should be considered as well since its molecules must have had some chemical reactions with the graphene platelets' surfaces affecting their intrinsic properties. To better understand the viscoelastic behaviour of the nanocomposite with regard to various frequencies, the

dynamic mechanical analysis (DMA) test must be considered. Also, to assess the thermal capacity of nanocomposites, differential scanning calirometry should be done. Furthermore, methods to increase the degree of exfoliation of the graphene nanoplatelets, as well as functionalization of their surface should be studied to improve the dispersion, adherence, and hence the mechanical properties and electrical conductivity of the nanocomposites without increasing the filler content.

REFERENCES

1. Anandhan, S., Bandyopadhyay, S., "Polymer Nanocomposites: From Synthesis to Applications", *INTECH Publication*, 2011.

2. Koo, J., H., *Polymer Nanocomposites: Processing, Characterization, and Applications*, McGraw-Hill, New York, 2006.

3. Mittal, V., *Polymer-graphene nanocomposites*, RSC Publication, 2012.

4. Mittal, V., *Advances in Polyolefin Nanocomposites*, CRS Press, 2010.

5. Tanahashi, M., "Development of Fabrication Methods of Fille/Polymer Nanocomposites: With Focus on Simple Melt-Compounding Based Approach without Surface Modification of Nanofillers", *Materials*, Vol. 3, pp. 1593-1619, 2010.

6. Geim, A. K., Novoselov, K. S., "The rise of graphene", *Nature Materials*, vol. 6, No. 3, pp. 183–191, 2007.

7. Khot, M., B., Gadekar, A., S., Kahane, M., J., Potnis, V., Baghwan, D., B., Dhamane, S., P., Kulkarni, A., S., "Graphene – A Review", *International Journal of Pharmaceutical and Phytopharmacological Research (eIJPPR)*, ISSN (Online) 2249-6084 (Print) 2250-1029.

8. Novoselov, K., S., Falko, V., I., Colombo, L., Gellert, P., R., Schwab, M., G., Kim, K., "A roadmap for graphene", *Nature*, Vol 490, 2012.

9. Zhou, C., Chen, S., Lou, J., Wang, J., Yang, Q., Liu, C., Huang, D., Zhu, T., "Graphene`s cousin: the present and future of graphene", *SpringerOpen Journal*, 2014.

10. Geim, A.K., "Graphene: Status and Prospects", *Science Journal*, Vol.324, No.5934, pp.1530-1534, 2009.

11. "Carbon Black User's Guide", *International Carbon Black Association*, 2016.

12. Krassowski, D.W., "Expandable Graphite Flake as an Additive for a New Flame Retardant Resin", *Graftech International*, 2012

13. Tamashausky, A.V., *Asbury Carbons*, 2016, *http://asbury.com/technical-presentations-papers/materials-in-depth/expandable-flake-graphite/*, accessed in January 2017

14. Vadukumpully, S., Paul, J., Valiyaveettil, S., ''Cationic srfactant mediated exfoliation of graphite into graphene flakes'', *Carbon*, Vol. 47, pp. 3288-3294, 2009.

15. Chabot, V., Kim, B., Sloper, B., Tzoganakis, C., Yu, A., ''High yield production and purification of few layer graphene by Gum Arabic assisted physical sonication'', *Scientific Reports*, Vol. 3, pp. 1378, 2013.

16. Lotya, M., King, P.J., Khan, U., De, S., Coleman, J.N., ''High-Concentration, Surfactant-Stabilized Graphene Dispersions'', *ACS Nano*, Vol. 4, No, 6, pp. 3155-3162, 2010.

17. He, H., Klinowski, J., Forster, M., Lerf, A., "A new structural model for graphite oxide", *Chemical Physics Letters*, Vol. 287, No. 1-2, PP. 53-56, 1998.

18. Brodie, F.R.S., "On the Atomic Weight of Graphite", *The Royal Society Publishing*, Vol. 149, pp. 249-259, 1859.

19. Staudenmaier, L., "Verfahren zur Darstellung der Graphitsäure", *European Journal of Inorganic Chemistry*, Vol. 31, pp. 1481-1487, 1898.

20. Hummers, W., S., Offeman, R., E., "Preparation of Graphite Oxide", *Journal of the American Chemical Society*, Vol 80, No.6, pp.1339-1339, 1958.

21. Dreyer, D.R., Park, S., Bielawski, C.W., Ruoff, R.S., "The chemistry of graphene oxide", *Journal of Chemical Society Review*, Vol. 39, pp. 228-240, 2010.

22. Loh, K.P., Bao, Q., Ang, P.K., Yang, J., "The chemistry of graphene", *Journal of Materials Chemistry*, Vol. 20, pp. 2277-2289, 2010.

23. Pei, S., Cheng, H.M., "The reduction of graphene oxide", *Carbon*, Vol. 50, pp. 3210-3228, 2012.

24. Schniepp, H.C., Li, J.L., McAllister M.J., Sai, H., Herrera-Alonso, M., Adamson, D.H., Prud`home, R.K., Car, R., Saville, D.A., Aksay, I.A., "Functionalized single graphene sheets derived from splitting graphite oxide", *The Journal of Physical Chemistry B*, Vol. 110, No. 17, pp. 8535-8539, 2006.

25. Li, X, Wang, H., Robinson, J.T., Sanchez, H., Diankov, G., Dai, H., "Simultaneous nitrogen doping and reduction of graphene oxide", *Journal of American Chemistry Society*, Vol. 131, No. 43, pp. 15939-15944, 2009.

26. Wang, X., Zhi, L., Mullen, K., "Transparent, conductive graphene electrodes for dye-sensitized solar cells", *Nano Letters*, Vol. 8, No. 1, pp. 323-327, 2008.

27. Stankovich, S., Dikin, D.A., Piner, D.R., Kohlhaas, K.A., Kleinhammes, A., Jia, Y., Wu, Y., Nguyen, S.T., Ruoff, R.S., "Synthesis of graphene-based nanosheets via chemical reduction of exfoliated graphite oxide", *Journal of Carbon*, Vol. 45, pp. 1558-1565, 2007.

28. Gomez-Navarro, C., Weitz, R.T., Bittner, A.M., Scolari, M., Mews, A., Burghard, M., Kern, K., "Electronic Transport Properties of Individual Chemically Reduced Graphene Oxide Sheets", *Nano Letters*, Vol. 7, No. 11, pp. 3499-3503, 2007.

29. Mattevi, C., Eda, G., Agnoli, S., Miller, S., Mkhoyan, K.A., Celik, O., Mastrogiovanni, D., Granozzi, G., Garfunkel, E., Chhowalla, M., "Evolution of Electrical, Chemical, and Structural Properties of Transport and Conducting Chemically Derived Graphene Thin Films", *Advanced Functional Materials*, Vol. 19, No. 16, pp. 2577-2583, 2009.

30. Li, D., Muller, M., Gilje, S., Kaner, R.B., Wallace, G.G., "Processable aqueous dispersions of graphene nanosheets", *Nature Nanotechnology*, Vol. 3, No. 2, pp. 101-105, 2008.

31. Fernandez-Merino, M.J., Guardia, I., Paredes, J.I., Villar-Rodil, S., Solis-Fernandez, P., Martinez-Alonso, A., Tascon, J.M.D., "Vitamin C Is an Ideal Substitute for Hydrazine in the Reduction of Graphene Oxide Suspensions", *Journal of Physical Chemistry C*, Vol. 114, pp. 6426-6432, 2010.

32. Stankovich, S., Pinar, R.D., Chen, X., Wu, N., Nguyen, S.T., Ruoff, R.S., "Stable aqueous dispersions of graphitic nanoplatelets via the reduction of exfoliated graphite oxide in the presence of poly (sodium 4-styrenesulfonate)", *Journal of Materials Chemistry*, Vol. 16, pp. 155-158, 2006.

33. He, Q., Wu, S., Gao, S., Cao, X., Yin, Z., Li, H., Chen, P., Zhang, H., "Transparent, flexible, all-reduced graphene oxide thin film transistors", *ACS Nano*, Vol. 5, No. 6, pp. 5038-5044, 2011.

34. Gilje, S., Han, S., Wang, M., Wang, K.L., Kaner, R.B., "A Chemical Route to Graphene for Device Applications", *ASC Nano Letters*, Vol. 7, No. 11, pp. 3394-3398, 2007.

35. Becerril, H.A., Mao, J., Liu, Z., Stoltenberg, R.M., Bao, Z., Chen, Y., "Evaluation of solution=processed reduced graphene oxide films as transparent conductors", *ACS Nano Letters*, Vol. 2, No. 3, pp. 463-470, 2008.

36. Li, X., Zhang, G., Bai, X., Sun, X., Wang, X., Wang, E., Dai, H., "Highly conducting graphene sheets and Langmuir-Blodgett films", *Nature Nanotechnology*, Vol. 3, No. 9, pp. 538-542, 2008.

37. Shin, H.J., Kim, K.K., Benayad, A., Yoon, S.M., Park, H.k., Jung, I., Jin, M.H., Jeong, H., Kim, J.M., Choi, J., Lee, Y.H., "Efficient Reduction of Graphite Oxide by Sodium Borohydride and Its Effect on Electrical conductance", *Advanced Functional Materials*, Vol. 19, pp. 1987-1992, 2009.

38. Gao, W., Alemany, L.B., Ci, L., Ajayan, P.M., "New insights into the structure and reduction of graphite oxide", *Nature Chemistry*, Vol. 1, No. 5, pp. 403-408, 2009.

39. Pei, S., Zhao, J., Du, J., Ren, W., Cheng, H.M., "Direct reduction of graphene oxide films into highly conductive and flexible graphene films by hydrohalic acids", *Carbon*, Vol. 48, No. 15, pp. 4466-4474, 2010.

40. Moon, K., Lee, J., Ruoff, R.S., Lee, H., "Reduced graphene oxide by chemical graphitization", *Nature Communications*, Vol. 1, No. 1, pp. 73-78, 2010.

41. Chetri, S., Kuila, Murmu, N., C., ''Graphene Composites'', *Wiley Online Library*, Online ISBN: 9783527687541, 2016.

42. Li, B., Zhong, W., H., '' Review on polymer/graphite nanoplatelet nanocomposites'', *Journal of Materials Science*, Vol.46, pp. 5595-5614, 2011.

43. Wang, J., Wang, X., Xu, C., Zhang, M., Shang, X., ‘’Preparation of graphene/poly (vinyl alcohol) nanocomposites with enhanced mechanical properties and water resistance’’, *Journal of Polymer International*, Vol. 60, pp. 816-822, 2011.

44. Liang, J., Huang, Y., Zhang, L., Wang, Y., Ma, Y., Guo, T., Chen, Y., ‘’Molecular-Level Dispersion of Graphene into Poly(vinyl alcohol) and Effective Reinforcement of their Nanocomposites’’, *Advanced Functional Materials*, Vol. 19, pp. 2297-2302, 2009.

45. Zhao, X., Zhang, Q., Chen, D., ‘’Enhanced Mechanical Properties Of Graphene-Based poly (vinyl alcohol) Composites’’, *Macromolecules*, Vol. 43, pp. 2357-2363, 2010.

46. Achaby, M., E., Qaiss, A., ‘’Processing and properties of polyethylene reinforced by graphene nanosheets and carbon nanotubes’’, *Materials and Design*, Vol. 44, pp. 81-89, 2013.

47. Inuwa, I., M., Hasan, A., Samsudin, S.A., Mohamad Haafiz, M.K., Jawaid, M., Majeed, K., Abdul Razak, N.C., ‘’Characterization and Mechanical Properties of Exfoliated Graphite Nanoplatelets Reinforced Polyethylene Terephthalate/Polypropylene Composites’’, *Journal of Applied Polymer Science*, Vol. 131, pp. 40582, 2014.

48. Abdul Razak, N.C., Inuwa, I.M., Hasan, A., Samsudin, S., ‘’Effects of compatibilizers on mechanical properties of PET/PP blend’’, *Composite Interfaces*, Vol. 20, No. 7, pp. 507-515, 2013.

49. Achaby, M., E., Arrakhiz, F., Vaudreuil, S., Qaiss, A., E., K., Bousmina, M., Fassi-Fehri, O., “Mechanical, thermal, and rheological properties of graphene-based polypropylene nanocomposites prepared by melt mixing”, *Polymer Composites*, Vol. 33, No. 5, pp. 733-744, 2012.

50. Li, Y.C., Chen, G.H., ‘’HDPE/Expanded Grapgite Nanocomposites Prepared via Masterbatch Process’’, *Polymer Engineering and Science*, Vol. 47, No. 6, pp. 882-888, 2007.

51. Wakabayashi, K., Pierre, C., Dikin, D.A., Ruoff, R.S., Ramanathan, T., Brinson, L.C., Tokelson, J.M., ‘’Polymer-Graphite Nanocomposites: Effective Dispersion and Major Property Enhancement via Solid-State Shear Pulverization’’, *Macromolecules*, Vol. 41, pp. 1905-1908, 2008.

52. Istrate, O., M., Paton, K., R., Khan, U., O`Neil, A., Bell, A., P., Coleman, J., N., “Reinforcement in melt-processed polymer-graphene composites at extremely low graphene loading level”, *Carbon*, Vol. 78, pp. 243-249, 2014.

53. Song, P., Cao, Z., Cai, Y., Zhao, L., Fang, Z., Fu, S., “Fabrication of exfoliated graphene-based polypropylene nanocomposites with enhanced mechanical and thermal properties”, Polymer, Vol. 52, pp. 4001-4010, 201154. Ma, P.C., Siddiqui, N.A., Marom, G., Kim, J.K., “Dispersion and functionalization of carbon nanotubes for polymer-based nanocomposites: A review”, *Composites: Part A*, Vol. 41, pp. 1345-1367, 2010.

54. Ma, P.C., Siddiqui, N.A., Marom, G., Kim, J.K., “Dispersion and functionalization of carbon nanotubes for polymer-based nanocomposites: A review”, *Composites: Part A*, Vol. 41, pp. 1345-1367, 2010.

55. Bao, S.P., Liang, G.D., Tjong, S.C., “Effect of mechanical stretching on electrical conductivity and positive temperature coefficient characteristics of poly(vinylidene flüoride)/carbon nanofiber composites prepared by non-solvent precipitation”, *Carbon*, Vol. 49, pp. 1758-1768, 2011.

56. Arjmand, M., Apperley, T., Okoniewski, M., Sundararaj, U., Park, S., "Comparative study of electromagnetic interference shielding properties of injection molded versus compression molded multi-walled carbon nanotube/polystyrene composites", *Carbon*, Vol. 50, pp. 5126-5134, 2012.

57. Jiang, M.J., Dang, Z.M., Bozlar, M., Miomandre, F., Bai, J.B., "Broad-frequency dielectric behaviours in multiwalled carbon nanotube/rubber nanocomposites", *Journal of Applied Physics*, Vol. 106, 084902, 2009.

58. Kuiper, P., *Comparison of the electronic band structures of metals, semiconductors and insulators*, 2007, *http://commons.wikimedia.org/wiki/File:Isolator-metal.svg*, accessed in January 2017.

59. Blythe T, Bloor D., *"Electrical properties of polymers"*, New York: Cambridge University Press, 2005.

60. Zhang, W., Dehghani-Sanij, A.A., Blackburn, R.S., "Carbon based conductive polymer composites", *Journal of Materials Science*, Vol. 42, pp. 3408-3418, 2007.

61. Miyasaka, K., Watanabe, K., Jojima, E., Aida, H., Sumita, M., Ishikawa, K., "Electrical conductivity of carbon-polymer composites as a function of carbon content", *Journal of Materials Science*, Vol. 17, pp. 1610-1616, 1982.

62. Sau, K.P., Chaki, T.K., Khastgir, D., "Conductive rubber composites from different blends of ethylene-propylene-diene rubber and nitrile rubber", *Journal of Materials Science*, Vol. 32, No. 21, pp. 5717-5724, 1997.

63. Sau, K.P., Chaki, T.K., Khastgir, D., "Carbon fiber filled conductive composites based on nitrile rubber, ethylene propylene diene rubber and their blend", *Polymer*, Vol. 39, No. 25, pp. 6461-6471, 1998.

64. Narkis, M., Vaxman, A., "Resistivity Behaviour of Filled Electrically Conductive Crosslinked Polyethylene", *Journal of Applied Polymer Science*, Vol. 29, No. 5, pp. 1639-1652, 1984.

65. Gubbels, F., Jerome, R., Teyssie, PH., Vanlathem, E., Deltour, R., Calderone, A., Parente, V., Bredas, J.L., "Selective Localization of Carbon Black in Immiscible Polymer Blends: A Useful Tool To Design Electrical Conductive Composites", *Macromolecules*, Vol. 27, No. 7, pp. 1972-1974, 1994.

66. Foulger, S.H., "Reduced percolation thresholds of immiscible conductive blends", *Journal of Polymer Science: Part B*, Vol. 37, No. 15, pp. 1899-1910, 1999.

67. Pramanik, P.K., Khastgir, D., Saha, T.N., "Conductive nitrile rubber composite containing carbon fillers: Studies on mechanical properties and electrical conductivity", *Composites*, Vol. 23, No. 3, pp. 183-191, 1992.

68. Pramanik, P.K., Khastgir, D., De, S.K., Saha, T.N., "Pressure-sensitive electrically conductive nitrile rubber composites filled with particulate carbon black and short carbon fibre", *Journal of Materials Science*, Vol. 25, No. 9, pp. 3848-3853, 1990.

69. Pramanik, P.K., Khastgir, D., Saha, T.N., "Effect of extensional strain on the resistivity of electrically conductive nitrile-rubber composites filled with carbon filler", *Journal of Materials Science*, Vol. 28, No. 13, pp. 3539-3546, 1993.

70. Zhang, Y.C., Dai, K., Tang, J.H., Ji, X., Li, Z.M., "Anisotropically conductive polymer composites with a selective distribution of carbon black in an in situ microfibrillar reinforced blend", *Materials Letters*, Vol. 64, pp. 1430-1432, 2010.

71. Zhang, H., B., Zheng, W., G., Yan, Q., Yang, Y., Wang, J., W., Lu, Z., H., Ji, G., Y., Yu, Z., "Electrically conductive polyethylene terephthalate/graphene nanocomposites prepared by melt compounding", *Polymer*, Vol.51, pp.1191-1196, 2010.

72. McAllister, M., J., Li, J., L., Adamson, D., H., Schniepp, H., C., Abdala, A., A., Liu, J., Herrera-Alonso, M., Milius, D., L., Car, R., Prud`homme, R., K., and Aksay, I., A., "Single Sheet Functionalized Graphene by Oxidation and Thermal Expansion of Graphite", *Chemistry of Materials*, Vol. 19, pp. 4396-4404, 2007.

73. Kuvardina, E., V., Novokshonova, L., A., Lomakin, S., M., Timan, S., A., Tchmutin, I., A., "Effect of the Graphite Nanoplatelet Size on the Mechanical, Thermal, and Electrical Properties of Polypropylene/Exfoliated Graphite Nanocomposites", *Journal of Applied Polymer Science*, Vol. 128, No. 3, pp. 1417-1424, 2013.

74. Verdejo, R., Bernal, M., M., Romasanta, L., J., Lopez-Manchado, M., A., "Graphene filled polymer nanocomposites", *Journal of Material Chemistry*, Vol. 21, pp. 3301-3310, 2011.

75. Grazon, C., Palza, H., "Electrical behavior of polypropylene composites melt mixed with carbon-based particles: Effect of the kind of particle and annealing process", *Composites Science and Technology*, Vol. 99, pp. 117-123, 2014.

76. Li. B., Zhong, W.H., "Review on polymer/graphite nanoplatelet nanocomposites", *Journal of Material Science*, Vol. 46, pp. 5595-5614, 2011.

77. Jenson, K., Mickelson, W., Kis, A., Zettl, A., "Buckling and kinking force measurements on individual multiwalled carbon nanotubes", *Physical Review B*, Vol. 76, No. 19, 195436, 2007.

78. Bellucci, S., "Carbon nanotubes: Physics and applications", *Physica Status Solidi (c)*, Vol. 2, No. 1, pp. 34-47, 2005.

79. Chae, H.G., Kumar, S., "Rigid Rod Polymeric fibers", *Journal of Applied Polymer Science*, Vol. 100, No. 1, pp. 791-802, 2006.

80. Sinnott, S.B., Andrews, R., "Carbon Nanotubes: Synthesis, Properties, and Applications", *Critical Reviews in Solid State and Materials Sciences*, Vol. 26, No. 3, pp. 145-249, 2001.

81. Adohi, B.J.-P., Mdarhri, A., Prunier, C., Haidar, B., Brosseau, C., "A comparison between physical properties of carbon black-polymer and carbon nanotubes-polymer composites", *Journal of Applied Physics*, Vol. 108, 074108, 2010.

82. Geim, A., K., "Graphene: Status and Prospects", *Science*, Vol. 324, No. 5934, pp. 1530-1534, 2009.

83. Soldano, C., Ather, M., Dujardin, E., "Production, properties and potential of graphene", *Carbon*, Vol. 48, pp. 2127-2150, 2010.

84. Singh, V., Joung, D., Zhai, L., Das, S., Khondakar, S., I., Seal, S., "Graphene based materials: Past, present and future", *Progress in Materials Science*, Vol 56, No. 8, pp. 1178-1271, 2011.

85. "Raman spectra and mechanical properties of graphene/PP nanocomposites'', *International Journal of Chemical Engineering and Application,* Vol. 6, No. 1, 2015.

86. Grafen Chemical Industries Co., *GRAFEN® -iGP2: Industrial Graphene Nanoplatelets for General Purposes,* 2013, *http://www.grafen.com.tr/pdf/1364466365.pdf,* accessed in January 2017.

87. Particle Sciences: Drug Development Services, "Hot Melt Extrusion Process", *Technical Brief,* Vol. 3, 2011.

88. ISO, "527-1 Plastics — Determination of Tensile Properties —Part 1: General Principles", *ISO 527-1,* 2012.

89. ASTM, "D1238-13 Standard Test Method for Melt Flow Rates of Thermoplastics by Extrusion Plastometer", *ASTM D1238,* 2013.